Trivedi and Puranik
Future Journal of Pharmaceutical Sciences (2023) 9:116
https://doi.org/10.1186/s43094-023-00559-0

Future Journal of Pharmaceutical Sciences

RESEARCH

Open Access

Chlorogenic acid-optimized nanophytovesicles: a novel approach for enhanced permeability and oral bioavailability

Hemangi R. Trivedi[1*] and Prashant K. Puranik[1]

Abstract

Background Chlorogenic acid, a phenolic derivative, shows excellent pharmacological properties. However, poor lipidic solubility, permeability, and oral bioavailability restrict its clinical use. Therefore, two different phospholipids—Phospholipon® 90H and LIPOID® S100 nanophytovesicles (NPVs)—were optimized, formulated and compared with central composite design for improved biopharmaceutical properties, antioxidant, anticancer and wound-healing activities.

Results Higher entrapment (> 95%) and partition coefficient values were obtained with optimized CGA 90H NPVs and S100 NPVs. Particle size and zeta potential values confirmed small particle size(≅ 450 nm) with optimum stability. Non-covalent interactions between CGA and both phospholipids were confirmed with Fourier transform infrared spectrophotometry, differential scanning calorimetry and proton nuclear magnetic resonance. NPVs significantly enhanced the lipidic solubility (> 25 times) supported by high-performance thin-layer chromatography. A sustained dissolution and diffusion release were obtained with NPVs as compared to pure CGA. Likewise, ≅ twofold increase in permeability was obtained, supported by confocal microscopy. Enhanced oral bioavailability of CGA with improved C_{max}, T_{max}, AUC, half-life values was obtained with NPVs along with *IVIV* correlation. Enhanced DPPH radical scavenging and Fe^{2+} chelation ability were obtained with CGA 90H NPVs > CGA S100 NPVs, with lower IC_{50} values in HeLa and HL-60 cell lines (< 0.75 times) as compared to CGA in MTT(3-(4,5-dimethylthiazol-2-yl)- 2,5- diphenyltetrazolium bromide) assay. Higher wound contraction percentages were observed at day 3 with CGA S100 NPVs (71.56%) > CGA 90H NPVs (34.0%) in wound-healing studies.

Conclusions The formulated NPVs exhibited efficiency of Phospholipon®90 H in enhancing oral bioavailability and LIPOID® S100 in increasing transdermal permeability, thus proving as promising carriers for enhancing biopharmaceutical and pharmacological properties of chlorogenic acid.

Keywords Chlorogenic acid, Phospholipon® 90H, LIPOID® S100, Nanophytovesicles, Central composite design, Solubility, Permeability, Oral bioavailability, Wound healing

Background

Chlorogenic acid, a phenolic derivative, shows wide availability in green coffee beans, all types of berries, apples, tubers and sunflowers [1, 2]. Also, it is a major phytoconstituent of many traditional medicinal plants such as *Solanum tuberosum* [3], *Loicera japonica* [4], *Cestrum nocturnum* L. [5], *Amaranthus Spinosus* [6], *Parrotia*

*Correspondence:
Hemangi R. Trivedi
hemangirtrivedi@gmail.com
Full list of author information is available at the end of the article

persica [7]. CGA produces abundant biological effects including anti-inflammatory [8], antidiabetic [9], antibacterial [10], anticancer [11], etc. Secondary polyphenolic molecule such as CGA reduces the free radicals and mitigates the oxidative stress. It also accentuates the synthesis of growth factors for tissue re-epithelization and thus is a potent antioxidant and wound-healing agent [12, 13]. Despite its effectiveness, CGA demonstrates low oral bioavailability and permeability (BCS class III), which is attributed to its hydrophilic nature (Log P ≅ − 1.44) and extensive metabolism into various metabolites like caffeic acid and quinic acid. Oral bioavailability studies with *Loicera Japonicae Flos* extract showed elimination half-life of CGA (≅ 48 min) in rat plasma [14]. Furthermore, CGA undergoes oxidation during improper storage or purification process [15]. Therefore, additional investigations are warranted to improve the physicochemical properties of CGA using a suitable nanodelivery system to achieve its potent therapeutic effect on target site.

Nanophytovesicles (NPVs) have been widely used to improve the physicochemical properties like bioavailability, permeability and stability of phytoconstituents. NPVs are primarily lipid biocompatible adducts based upon the affinity of drug molecule for phospholipids via hydrogen bonding, dipole–dipole interactions or van der Waals forces [16]. This complexation has shown incredible potential against other delivery systems with avoidance of first pass metabolism, sustained and controlled release, higher entrapment, and overall increased physical and chemical stability. Many research groups have adopted different strategies to overcome the CGA-associated challenges including phospholipid complexation and advocated its protective action against UVA (long-wave ultraviolet A)-induced oxidative stress [17] and post-MI (*Myocardial infarction*) inflammatory effects [18]. Other study groups also reported film drying liposomal encapsulation [19] and chitosan nanoparticles [20]. However, after careful review of the published reports, we noticed that authors majorly addressed antioxidant potential of CGA without addressing CGA solubility, permeability, oral bioavailability with higher entrapment, stability, wound-healing properties or cell-based assays. Thus, based on these shortcomings of studies, we have reported optimized and promising CGA NPVs with enhanced lipidic solubility, permeability, oral bioavailability, wound-healing activity and cell viability.

NPVs are comprised of drug moiety and phospholipids. In our study, we compared the efficiency of two different phospholipids—Phospholipon® 90H and Lipoid® S100. These phospholipids differ in their hydrogenation content and are widely used for oral and transdermal delivery systems [21]. These phospholipids interact with the bilayers of cell membrane and facilitate transportation of the NPVs across the membrane in a protective fashion. The intermolecular association between polar groups of drug moiety and choline group present in the phospholipids yields a stable, efficient and amphiphilic NPVs, which enhance permeability and bioavailability [22]. In the present work, it was hypothesized that Phospholipon® 90H and Lipoid® S100 would establish intermolecular association with polar groups of CGA, forming CGA 90H NPVs and CGA S100 NPVs resulting in enhanced solubility, permeability, bioavailability along with efficient wound healing and cell viability potential of CGA. Also, in this study, NPVs were developed and optimized using solvent evaporation method with central composite experimental design to understand the impact of process and material variables. The optimized NPVs were evaluated for their solubility using partition coefficient values and high-performance thin-layer chromatography, particle size, entrapped drug, zeta potential, Fourier transform infrared spectroscopy, differential scanning calorimetry and proton nuclear magnetic resonance. They were further characterized morphologically by transmission electron microscopy and functionally by in vitro dissolution, ex vivo permeation and in vivo oral bioavailability studies. Additionally, antioxidant assays, cell viability assay and wound-healing potential of NPVs were tested using excision wound model in rats.

Methods

Materials

CGA was obtained from Chemsworth, India. Soyabean phospholipid LIPOID® S100 and hydrogenated phospholipid Phospholipon® 90H were obtained as gratis samples from Lipoid, Germany. DPPH (2-diphenyl-1-picrylhydrazyl), ferrozine and ferric chloride were obtained from SD fine chemicals, India. Dichloromethane and N-hexane were purchased from Merck, India. Rhodamine 6G and sinapic acid (Internal standard) D7927 were procured from Sigma-Aldrich, USA. Silverex® heal hydrogel (1% colloid silver) (Sun pharmaceuticals In. Ltd.) was purchased from local pharmacy shop. MTT(3-(4,5-dimethylthiazol-2-yl)- 2,5- diphenyltetrazolium bromide) was purchased from Thermo Fisher scientific, India. MEM (Minimum Essential Medium Eagle) and RPMI-1640 (Roswell Park Memorial Institute) medium, foetal bovine serum (FBS) were obtained from HiMedia Lab, India. While all other reagents used in the study were of analytical grade. HL-60 (human leukaemia cell line) and HeLa (Henrietta Lacks cervical cancer cell line) were obtained from National Centre for cell lines, India.

Formulation and optimization of CGA NPVs (CGA 90H NPVs and CGA S100 NPVs) by central composite design (CCD)

CGA 90H NPVs and CGA S100 NPVs were formulated and optimized using central composite experimental design, which gave 20 different combinations of experimental batches with three independent factors (drug phospholipid ratio, reaction time and reaction temperatures) at three different levels (−1, 0, +1) with additional extreme low–high levels (−1.68, +1.68). NPVs were prepared using the widely employed solvent evaporation technique [21]. Briefly, CGA and phospholipid (Phospholipon® 90H /Lipoid® S100) were weighed as per their molar ratios (1:0.3, 1:1, 1:2, 1:3 and 1:3.6) (X_1, w: w) and transferred to a round-bottom flask (100 mL). To this aprotic solvent (dichloromethane 20 mL) was added and refluxed at different reaction temperatures (33.1, 40, 50, 60 and 66.8 °C) (X_3, °C) at different reaction times (0.31, 1, 2, 3 and 3.6 h) (X_2, h). After completion, the mixture was reduced to 3–4 mL concentrate residue, which was further precipitated with n-hexane to yield NPVs. The precipitate was allowed to stand at room temperature for evaporation of n-hexane for 24–48 h. The dried NPVs were weighed in order to calculate yield and stored in a glass bottle at ambient temperature. The yield of CGA NPVs (%) is calculated using Eq. 1 where A is the amount of CGA NPVs obtained and B is total of reaction dosage used.

$$\text{Yield} = \frac{A}{B} \times 100 \tag{1}$$

The dependent particulars for both NPVs are given in Table 1. The data obtained were computed and analysed using Design expert® software (Version 11.1.2.0, Stat-Ease, Inc, Minneapolis). The polynomial equation generated (Eq. 2) gives the interaction and impact of different material and process variables over one another and also on partition coefficient(Y_1) and entrapment efficiency(Y_2) of final formulation.

$$\begin{aligned} Y =& b_0 + b_1X_1 + b_2X_2 + b_3X_3 + b_{11}X_1^2 \\ &+ b_{22}X_2^2 + b_{33}X_3^2 + b_{12}X_1X_2 \\ &+ b_{23}X_2X_3 + b_{13}X_1X_3 \end{aligned} \tag{2}$$

Herein, X_1 X_2 X_3 are the independent factors, X_1X_2, X_2X_3, X_1X_3 are the interaction terms and ${X_1}^2$, ${X_2}^2$, ${X_3}^2$ are the polynomial terms. Further, validation of the generated

Table 1 Experimental runs and their observed responses for CGA 90H NPVs and CGA S100 NPVs using central composite design

Batch	X_1	X_2	X_3	CGA 90H NPVs			CGA S100 NPVs		
				Y_1*	Y_2*	*PY**	Y_1*	Y_2*	*PY**
F1	2	2	50	0.954 ± 0.04	69.02 ± 0.51	90.2 ± 0.12	0.702 ± 0.52	85.46 ± 0.63	83.78 ± 0.01
F2	3	1	40	0.778 ± 0.61	68.5 ± 0.68	82.7 ± 0.16	0.580 ± 0.15	86.69 ± 0.08	60.9 ± 0.18
F3	2	2	50	0.841 ± 0.42	75.93 ± 0.19	97.5 ± 0.43	0.710 ± 0.67	82.64 ± 0.19	81.14 ± 0.93
F4	2	3.68	50	0.798 ± 0.59	83.45 ± 0.29	98.2 ± 0.23	0.560 ± 0.23	88.0 ± 0.74	85.8 ± 0.64
F5	2	2	50	1.036 ± 0.12	81.41 ± 0.37	94.5 ± 0.21	0.734 ± 0.45	81.69 ± 0.38	86.7 ± 0.56
F6	2	2	50	0.719 ± 0.22	78.45 ± 0.91	92.0 ± 0.45	0.729 ± 0.28	83.12 ± 0.56	81.7 ± 0.38
F7	**1**	**1**	**60**	0.492 ± 0.53	69.69 ± 0.49	82.7 ± 0.13	**0.947 ± 0.01**	**87.89 ± 0.68**	**94.6 ± 0.16**
F8	2	2	66.8	0.435 ± 0.99	75.44 ± 0.04	89.8 ± 0.18	0.857 ± 0.18	85.93 ± 0.82	79.6 ± 0.18
F9	1	3	40	0.653 ± 0.58	73.72 ± 0.06	87.6 ± 0.21	0.628 ± 0.28	87.94 ± 0.73	79.6 ± 0.70
F10	0.31	2	50	0.502 ± 0.61	71.82 ± 0.33	82.9 ± 0.10	0.674 ± 0.10	87.91 ± 0.12	81.5 ± 0.22
F11	1	3	60	0.693 ± 0.01	64.6 ± 0.35	81.8 ± 0.33	0.631 ± 0.37	87.89 ± 0.34	85.2 ± 0.43
F12	2	2	50	0.687 ± 0.88	80.5 ± 0.82	94.4 ± 0.76	0.756 ± 0.43	81.14 ± 0.93	80.7 ± 0.19
F13	2	2	50	0.735 ± 0.11	77.25 ± 0.59	93.8 ± 0.50	0.731 ± 0.28	85.78 ± 0.01	78.0 ± 0.63
F14	2	0.31	50	0.922 ± 0.36	72.27 ± 0.29	92.6 ± 0.14	0.888 ± 0.45	81.45 ± 55	86.8 ± 0.55
F15	3	3	40	0.835 ± 0.72	66.13 ± 0.17	77.2 ± 0.71	0.835 ± 0.72	66.13 ± 0.17	83.7 ± 0.21
F16	3.68	2	50	0.592 ± 0.53	82.47 ± 0.18	93.3 ± 0.88	0.632 ± 0.47	85.68 ± 0.29	83.1 ± 0.12
F17	2	2	33.1	0.662 ± 0.77	74.47 ± 0.13	94.2 ± 0.81	0.832 ± 0.84	80.05 ± 0.91	82.4 ± 0.19
F18	3	3	60	0.546 ± 0.10	81.81 ± 0.37	93.3 ± 0.18	0.871 ± 0.88	82.02 ± 0.49	86.8 ± 0.46
F19	1	1	40	0.354 ± 0.45	84.01 ± 0.23	68.2 ± 0.38	0.765 ± 0.38	77.85 ± 0.16	81.3 ± 0.56
F20	**3**	**1**	**60**	**0.977 ± 0.53**	**96.89 ± 1.22**	**97.2 ± 0.28**	0.678 ± 0.22	85.43 ± 0.88	73.1 ± 0.80

Optimized batch values are highlighted

X_1: Drug: PHOSPHOLIPON® 90H/Lipoid® S100 ratio (w/w); X_2: Reaction time; X_3: Reaction temperature (°C), Y_1: Partition coefficient, Y_2: Entrapment efficiency (%), *PY*: Per cent yield (%)

* Data were represented as mean ± SD ($n = 3$)

value was carried out by preparing a check point formulation using optimal values predicted by the model. The error or bias of the obtained model was determined using the formula-

$$\text{Bias}(\%) = \frac{\text{predicted value} - \text{observed values}}{\text{predicted value}} * 100 \quad (3)$$

Characterization of CGA NPVs

Partition coefficient of CGA 90H NPVs and CGA S100 NPVs was determined using the widely employed shake flask method [23]. Briefly, the preweighed NPVs were (-10 mg) taken in conical flask (100 mL) to which 10 mL of distilled water and n-octanol were added. These flasks were then subjected to rotary shaker (REMI RS-12 plus, Mumbai). After 24 h, the mixtures were transferred to separating funnels and further allowed to stand for 30 min so that both water and octanol phases separate. The amount of CGA partitioned between the phases was then determined using UV spectrophotometer (Jasco (V-630), Japan) ($n=3$). The concentration of CGA was determined using calibration curve equation and further incorporated in the following equations to obtain partition coefficient and Log P values.

$$\text{Log}P = \text{log10(Partition coefficient)} \quad (4)$$

$$\text{Partition coefficient} = \frac{Co}{Cw} \quad (5)$$

where C_o – concentration in n-octanol phase, C_w – Concentration in water phase. While entrapped CGA in NPVs was determined using earlier reported methods [24] for which dried NPVs(− 10 mg) were accurately weighed in beakers(100 mL) to which 6.8pH phosphate buffer was added (− 50 mL). It was then subjected under continuous stirring on a magnetic stirrer. After 4 h, the beaker was allowed to stand still (1 h) and the clear liquid obtained was decanted, while the sludge was centrifuged (Remi C24 plus, India) at 5000 rpm (15 min). The supernatant obtained was filtered (0.4 µm Whatman filter paper) and subsequently diluted and analysed in UV spectrophotometer (Jasco (V-630), Japan) (λmax = 323.8 nm).

$$\text{Drugentrapped} = \left\{ \frac{\text{Total amount of CGA in formulation} - \text{Amount of free CGA obtained}}{\text{Total amount of CGA in formulation}} * 100 \right\} \quad (6)$$

Further, dynamic light scattering technology was employed to determine NPVs size distribution, polydispersity index and their zeta potential values using Zetasizer® Nano (Malvern Instruments (Nano- ZS90), Massachusetts, USA). Morphological characterization of both NPVs was carried out using transmission electron microscopy (Joel, JM 2100) [22].

Fourier transform infrared spectroscopy (FTIR)

FTIR technique was employed to determine the presence of different functional groups present in CGA and phospholipids and also to study any interaction between them. Samples of pure CGA along with both phospholipids (Phospholipon® 90H /Lipoid® S100), physical mixtures and optimized NPVs formulations were analysed using FTIR spectrophotometer (Shimadzu-IRAFFINITY-1, Japan). All the samples were scanned in the range of 4000 to 400 cm^{-1} (FTIR 1-S Affinity Shimadzu, Japan) with DLATGS detector [25].

Differential scanning calorimetry (DSC)

DSC was employed to identify thermal changes caused by change in the physicochemical properties of NPVs as a function of temperature and time. The sample of pure CGA, both phospholipids (Phospholipon® 90H /Lipoid® S100), their physical mixtures and optimized NPVs were weighed (~ 5 mg) and placed in hermetically sealed pan in detector (DSC 60 PLUS, Shimadzu, Japan) under flowing nitrogen gas (100 mL/ min) and heating rate of 5 °C/min from 0 to 300 °C. The thermograms obtained were analysed using TA-60 software [26].

High-performance thin-layer chromatography (HPTLC)

Silica gel 60 F254 (E. MERCK KGaA, 5×10 cm) was used as stationary phase and ethyl acetate/water/formic acid/toluene (20:2:2:1) was used as a mobile phase with solvent upfront position of 92 mm. Hamilton syringe (100µL) was used for application of samples (5µL and 10 µL), while the detection of Rf values was carried out using CAMAG TLC scanner (scanning speed 20 mm/s with 100 µm/step resolution)using D2 lamp (273 V) and data filtration through Savitzky–Golay 7. The data were computed through WinCats planar software [27].

^{1}H-NMR analysis

The ^{1}H-NMR analysis was carried out to determine the carbon–hydrogen relationships between the CGA molecule and formulation excipients. Pure CGA and CGA NPV formulations were analysed by dissolving ≅ 10 mg of sample in 0.5 mL of chloroform in a clean NMR tube. The tube was sealed and ultrasonicated to ensure complete

dissolution. Spinner was placed in a sample depth gauge to ensure proper placement of NMR tube. The analysis was carried out on NMR spectrophotometer (Bruker Advance III 400 MHz) at 100 k [28].

In vitro dissolution studies

The dissolution behaviours of CGA NPVs were analysed and compared with pure CGA using dialysis bag method [29]. Briefly, a dialysis membrane (LA 390, Dialysis membrane 60, average diameter 15.9 mm, average flat width 25.27 mm and capacity ~ 1.99 mL/cm; High media lab, Mumbai) having the ability to retain molecules > 12,000 kDa was used to prepare dialysis bags for the study. The membrane was priorly activated using 2% sodium bicarbonate and 1 mM of EDTA solution at 80 °C for 30 min [30]. A 2 mL of CGA suspension (4 mg/mL)/ CGA NPVs suspension (~ 4 mg/mL of CGA) was poured in the dialysis bag and tied. The toffee tied dialysis bag was suspended into a beaker (250 mL) containing phosphate buffer medium (pH 6.8). The beaker was then subjected to magnetic stirring at 50 rpm at 37 ± 1 °C. Drug release was determined over the period of 24 h by removing aliquots from dissolution medium and running it in UV–Vis spectrophotometer (Jasco (V-630), Japan) at 323.8 nm ($n = 3$).

Formulation of NPVs hydrogel

Optimized NPVs were incorporated into Carbopol 934 hydrogel matrix by employing cold mechanical method in order to develop a secondary hydrogel formulation. Briefly, 1% Carbopol 934 powder was dispersed onto 100 mL of distilled water and refrigerated (2–8 °C) for 24 h. To this dispersion was added ethanolic solution of CGA and CGA NPVs(~ 1%w/v) along with propylene glycol (12.50%w/v) and triethanolamine (0.50%w/v to 6-7pH) with continuous stirring [31].

Characterization of NPVs hydrogel

To determine the applicability of the formulated hydrogel, viscosity was measured with Brookfield viscometer (Rotational viscometer, Viscolead one, Fungilab S.A., software version 1.2).A weighed amount of hydrogel (≅ 25 g) was taken in a beaker (50 mL), spindle (no 4) was dipped into the hydrogel and viscosity was recorded with different rpms at room temperature.The hydrogel was also analysed for its drug content by dissolving hydrogel(1 g) in 10 mL methanol with analysis using UV–Vis spectrophotometer at 328.2 nm ($n = 3$) along with pH determination (Digital pH metre, Systronics) [31]. Compatibility was further evaluated with skin irritation study using Draize patch test with adult Sprague Dawley rats (220 ± 5.69 g). Briefly, rats were segregated into five different groups after shaving their dorsal region using electric trimmer (Philips, India) 12 h prior to the protocol. Group I received the negative control (blank Carbopol gel), Group II received standard irritant 0.8% (v/v) formalin solution as positive control. Group III received 1% CGA Carbopol hydrogel while group IV and V received CGA 90H NPV and CGA S100 NPV hydrogels. The treatment was continued for three days and observed for signs of oedema or erythema [32].

Drug diffusion and permeation study

In vitro drug diffusion and ex vivo drug permeation studies were carried out for CGA NPVs hydrogel and compared with CGA hydrogel using a 6 station Franz diffusion apparatus (Orchid scientific (EMFDC-06), Nashik) with diffusion area of 2.01 cm^2. In vitro drug diffusion study was carried out by securing the activated dialysis membrane between the donor and the recipient compartment with no bubbles present between them. While for ex vivo drug permeation study, dorsal skin of Sprague–Dawley rats was obtained, the dermal region was depilated and cleaned of any attached subcutaneous tissue or blood vessels and stored in deep refrigeration (− 18 °C) until use. On the day of protocol, rat skin tissue was thawed and equilibrated by immersion in phosphate buffer (pH 7.4). The skin Sect. (2 × 2 cm) was fixed between donor and recipient compartment. The donor compartment was loaded with CGA and CGA NPV hydrogels (~ 4 mg of CGA), while the recipient compartment was maintained at 37 ± 1 °C with constant stirring by a Teflon-coated magnetic beads (100 rpm). At specific time periods (30 min, 1 h, 2 h, 4 h, 6 h, 8 h, 10 h, 24 h, 28 h, 32 h and 48 h), aliquots were withdrawn with maintenance of sink condition. The amount of drug diffused was measured at 323.6 nm with UV–Vis spectrophotometer (Jasco (V-630), Japan) by using 7.4pH phosphate buffer as blank. The kinetics and mechanism of drug diffusion were studied by plotting the data in various models [33] along with calculation of release rate constants (k) and correlation coefficient (R^2). While the cumulative amount of drug permeated over the period of 48 h was determined in terms of steady-state flux, permeability coefficient, enhancement in flux ratio and percentage of cumulative drug permeated [34]. Data < P 0.005 were considered statistically significant.

$$\text{Steady state flux(Jss)} = \frac{\text{Amount of drug permeated}}{(\text{time} * \text{diffusion membrane area})} \quad (7)$$

$$\text{Permeability Coefficient}(K\text{p}) = \frac{\text{Flux(Jss)}}{\text{Initial concentration of drug loaded in donor chamber}} \quad (8)$$

$$\text{Enhancement Ratio(ER)} = \frac{\text{Jss of vesicular hydrogel}}{\text{Jss of CGA hydrogel}} \quad (9)$$

$$\text{Percent cumulative permeated} = \frac{\text{Amount of drug permeated}(\mu\text{g/cm2})}{\text{Initial concentration of drug loaded in donar chamber}} * 100 \quad (10)$$

To further corroborate the permeation ability of CGA and CGA NPVs hydrogel, confocal fluorescence microscopy (CLSM) was carried out with Rhodamine 6G (RHO) (0.03%) labelling. CGA RHO hydrogel(standard) and CGA NPVs RHO hydrogels [35] were compared using Franz diffusion cell (as explained in ex vivo permeation study). After completion of 8 h, the skin was washed with phosphate buffer (pH 7.4) and treated with 4% paraformaldehyde solution overnight with refrigeration in order to fix the dye [36]. The skin tissues were further stored in sucrose solution as cryoprotectant until sectioning. A 5-µm-thick sections were cut using microtome (Leica, Germany) and examined under tandem confocal scanning SP5II microscope (Leica microsystems Ltd.) with dry objective lens (10X/0.30). Skin specimen was excited (area 1.48 mm^2) by employing Argon laser (20% power, emission bandwidth at 580–660 nm). Fluorescence emitted by RHO was obtained as red band at 594 nm (Leica LASX software).

Stability study

Long-term stability testing was carried out for optimized CGA 90H NPV and CGA S100NPV by determining any changes in their partition coefficient, entrapment efficiency and zeta potential values. The optimized batches were stored in glass vials at two different temperature conditions (25 °C ± 2 °C/60% RH ± 5% RH & 2–8 °C) and evaluated at specific time intervals over the period of 6 months (0,3,6 month) [37]. The formulated topical hydrogels were also examined for any changes in pH and drug content at refrigerated conditions (0,1,2 and 3 months).

In vitro antioxidant study

Two different assay techniques were employed to determine the antioxidant potential of CGA NPVs and compare them with pure CGA. DPPH radical scavenging assay was employed to determine the ability of CGA to reduce 0.2 mM DPPH (1 mL) and compare it with CGA NPVs (20–200 µg/mL in methanol). The reaction mixture in a stoppered test tube was allowed to stand in dark (30 min) with intermittent shaking. The per cent radical scavenged was determined by measuring absorbance at 517 nm with UV–Vis spectrophotometer (Jasco (V-630), Japan) using DPPH solution as blank [38]. Subsequently, Fe^{2+} chelation ability was determined by mixing CGA or CGA NPVs (20–200 µg/mL in methanol) and mixture of 5 mM of Ferrozine and 2 mM of ferric chloride in stoppered test tube. The reaction mixture was further stored in dark (10 min) and then absorbance measured with UV–Vis spectrophotometer (Jasco (V-630), Japan) at 562 nm by using a mixture of ferrozine, ferric chloride and methanol (0.25:0.25:1.75 mL) as blank [39].

$$\%\text{DPPH radical scavenging activity} = \frac{(\text{Ac} - \text{At})}{\text{Ac}} * 100 \quad (11)$$

$$\text{Ferrous ion chelation}(\%) = \frac{(\text{Ac} - \text{At})}{\text{Ac}} * 100 \quad (12)$$

where A_c is absorbance of control and A_t is Absorbance of test sample. Data $P < 0.005$ were considered to be statistically significant.

Cell viability study

The anticancer potential of CGA NPVs in comparison with pure CGA was evaluated using MTT tetrazolium cell viability assay on 2 cell lines—HL-60 [40] and HeLa [41]—by modifying the method. A standard stock solution of CGA was prepared (7.5 mg in 1 mL PBS of pH 6.8), which served as the positive control, and similarly CGA 90H NPV and CGA S100 NPV stock solutions (~7.5 mg in 1 mL PBS of pH 6.8) were prepared. Briefly, HeLa and HL-60 cells were seeded at 5×10^3 in 200 µL per well of MEM and RPMI 1640 medium, respectively, with 10% FBS, 100 units/mL penicillin and 100 µg/mL streptomycin in a 96-well TC plate (37 °C in 5% CO_2). After 24 h of incubation, both the cells were exposed to different concentrations of CGA and CGA NPVs (0.2, 0.4, 0.8, 1.1, 1.5, 1.9, 2.3, 2.6, 3.0, and 3.4 mg/ml) for 48 h (37 °C in 5% CO_2). HeLa cells were washed with PBS to remove any spent media and then directly exposed to MTT in fresh media with further incubation of 4 h. While with HL-60 cells, a cell sediment was obtained after centrifugation

(900 g) which was washed and resuspended in fresh medium with MTT supplementation and further incubation of 4 h. The protocol was repeated in triplicate, and the absorbance was determined by microplate reader at 570 nm (Bio-Rad, Hercules, CA, USA). Percentage cell viability is calculated (Eq. 13) and expressed as per cent of control cells, which were not treated [42]. The data obtained were statistically analysed and reported as mean ± SD, while the IC_{50} values were calculated using excel worksheet processor. Data $P < 0.005$ were considered to be statistically significant.

$$\%\text{Cell viability} = \frac{\text{Optical density of treated cells (mean)}}{\text{Optical density of control cells (mean)}} * 100 \quad (13)$$

Pharmacodynamic study: wound healing in excision wound rat model

Animals

Albino Sprague–Dawley rats were weighed (220 ± 5.69 g), segregated in 5 different groups and marked for identification ($n = 5$). Group I were treated topically with blank Carbopol hydrogel as negative control, while Group II received Silverex® heal marketed hydrogel as positive control. Group III were treated topically with CGA hydrogel (1%), and groups IV and V received CGA 90H NPV and CGA S100 NPV hydrogels, respectively.

Excision wound model

Thoracic dermal region of rats was depilated using inhalational anaesthesia (diethyl ether) [43], 24 h before the protocol. One excision wound was created per animal by removing ~ 200 mm^2 full thickness skin. The wound was treated with PBS and left undressed to open environment [44]. CGA and CGA NPVs hydrogel along with the positive and negative control hydrogels were applied topically once daily till the wound healed completely. The healing was monitored for 15-day period by measuring the wound area at specific time points (0, 3, 6, 9, 12, and 15th day with Vernier calliper). The wound was considered to be healed when there was regrowth of epithelium over granulation tissue. The wound healing was studied further with histopathological study of skin specimens isolated from one animal per group on 6th and 12th day of the study period. The isolated skin specimens were fixed in 10% formalin and sectioned (5 µm) using paraffin wax block. Staining was carried out with haematoxylin–eosin dye and viewed under microscope (Leica, DM2000 LED, X200) for studying the skin structures like fibroblasts, collagen formation and growth of epithelial layer [3]. The data were presented as mean ± standard deviation (SD) for each group ($n = 5$). All the data were analysed by employing Student's t-test to determine the efficiency of CGA NPV formulation groups over the positive/negative control groups [45]. Data $P < 0.05$ were considered to be statistically significant.

Pharmacokinetic study: In vivo oral bioavailability studies

Animal selection, dosing and blood collection

Healthy Sprague–Dawley rats (220 ± 5.69 g) were segregated and marked for identification in different groups ($n = 5$). Single-dose parallel group design [46] was used with 12 h fasting prior to the dosing. Group I was control group, which received no treatment, while group II received oral CGA suspension (100 mg/kg). Groups III and IV received CGA 90H NPV and CGA S100 NPV suspension (~ 100 mg/kg) orally using oral gavage feeding needle. At predetermined time intervals (0.08, 0.25, 0.5, 0.75, 1, 2, 4, and 8 h), blood samples (0.5 mL) were collected from the retro orbital vein in Eppendorf microcentrifuge tubes. The blood samples were then centrifuged (Remi C-24 plus, India) at 3500 rpm for 10 min, and the obtained plasma was stored under deep refrigeration (-20 °C) until HPLC analysis.

Chromatographic sample processing

High-performance liquid chromatography (HPLC) instrument (Agilent (1100) gradient system, USA) with UV detector (G1314A) and ISO pump (G1310A) equipped with CHMSTATION software for data analysis was used. A reverse phase C18 column (4.6 mm × 150 mm, 5 µm) with mobile phase (90:10, 0.05% orthophosphoric acid: acetonitrile) flowing at a rate of 1 mL/ min at 325 nm detection wavelength was employed. For determining CGA in rat plasma, to blood plasma (160 µL) was added 20µL of internal standard Sinapic acid (100 µg/10 mL) [47] in Eppendorf microcentrifuge tube. Subsequently (400µL) acetonitrile was added to precipitate plasma protein with further centrifugation (Remi C-24 plus, India) at 3500 rpm for 10 min. The supernatant obtained was filtered through membrane filter (0.2 µm membrane filter, Thermo Fisher Scientific, India.) before column injection.

Pharmacokinetic parameters and IVIVC correlation

Different pharmacokinetic parameters like maximum plasma concentration (C_{max}) and time required to reach maximum concentration (T_{max}) were obtained from concentration time curve directly. The remaining parameters like half-life($t_{1/2}$), area under the plasma concentration time curve ($AUC_{0\text{-}t}$), mean residence time (MRT), clearance (cl/F), volume of distribution (Vz/F), and relative bioavailability (F) were calculated using PK solver

software. Additionally, model-independent Wagner–Nelson method was employed to intercorrelate in vitro drug release and in vivo drug absorbed from CGA and CGA NPVs for 8 h. The data obtained were plotted and overlayered for correlation. The per cent drug absorbed in vivo was calculated using the Wagner–Nelson method where elimination rate constant K was obtained from slope of plasma drug concentration versus time plot, $(XA)_t/(XA)_\infty$ is the amount of drug absorbed, Cp denotes the plasma drug concentration at time t, $(AUC)_0^t$ was area under the curve from time 0 to t and $(AUC)_0^\infty$ was area under the curve from 0 to infinity:

$$\frac{(XA)t}{(XA)\infty} = \frac{Cp + K(AUC)_0^t}{K(AUC)_0^\infty} \tag{14}$$

All the data were analysed by employing one-way analysis of variance and Student's t test to determine the difference between formulation groups and positive/negative control groups. Data were considered statistically significant at $P < 0.005$.

Results

Mathematical modelling and optimization

The central composite design gave 20 different batches of CGA 90H NPVs and CGA S100 NPVs showing the obvious effect of independent variables on the dependent variables (Table 1). Batch F20 CGA 90H NPVs was the optimized batch with the highest partition coefficient (0.977 ± 0.53) and entrapment efficiency (99.6 ± 0.17%). Similarly, F7 of CGA S100 NPVs was the most efficient batch with the highest partition coefficient value (0.947 ± 0.01) and entrapment efficiency value (87.89 ± 0.68%). Also, the per cent yield of CGA obtained with CGA 90H NPV was 97.2 ± 0.28% and 94.6 ± 0.16% with CGA S100 NPV. These optimized batches were further used for all the studies. The data obtained was computed in Design expert software to generate quadratic polynomial mathematical equations for partition coefficient (Y_1) and entrapment efficiency (Y_2) of CGA NPVs:

CGA 90H NPVs

$$\begin{aligned} Y_1 =& 0.8279 + 0.0802X_1 - 0.0060X_2 - 0.0215X_3 - 0.1092X_1X_2 \\ & - 0.0335X_1X_3 - 0.0732X_2X_3 - 0.0943X_1^2 + 0.0163X_2^2 \\ & - 0.0938X_3^2\left(R^2 = 0.8340; P = 0.0480\right) \end{aligned} \tag{15}$$

$$\begin{aligned} Y_2 =& 76.53 + 3.07X_1 - 1.23X_2 \\ & + 1.83X_3 - 0.5975X_1X_2 + 8.78X_1X_3 \\ & - 1.28X_2X_3\left(R^2 = 0.7810; P = 0.0100\right) \end{aligned} \tag{16}$$

CGA S100 NPVs

$$\begin{aligned} Y_1 =& 0.6921 - 0.0025X_1 - 0.0375X_2 \\ & + 0.0232X_3 + 0.1181X_1X_2 \\ & + 0.0543X_3^2\left(R^2 = 0.8573; P = 0.0127\right) \end{aligned} \tag{17}$$

$$\begin{aligned} Y_2 =& 84.87 - 0.6114X_1 + 1.01X_2 \\ & + 1.30X_3 - 2.17X_1X_2 - 1.51X_1X_3 \\ & - 1.20X_2X_3\left(R^2 = 0.7372; P = 0.0347\right) \end{aligned} \tag{18}$$

The equations exhibit the synergistic (positive sign) and antagonistic (negative) effect of independent factors along with their interaction terms and polynomial terms on the dependent factors.

Validation of the generated model

The polynomial equations and 3D plots generated from the software indicated the optimized time and temperature along with appropriate amounts of phospholipid required to formulate stable NPVs (Fig. 1). The optimized model obtained from design expert software was validated by further formulating a check point batch using the graphical and numerical optimization and overlay plots (Fig. 2A &B). Evaluation of all the independent variables at different levels was carried out over the desired dependent variables given in the overlay plot. The predicted and observed values obtained for both the NPVs did not show major differences highlighting the robustness, while low bias values indicated validity of the experimental design (Table 2).

Characterization of CGA 90H NPVs and CGA S100 NPVs

A significant increase in Log P value ($P < 0.05$) was obtained with CGA 90H NPVs (− 0.01) and CGA S100 NPVs (− 0.02) as compared to pure CGA (− 1.44) highlighting the increase in lipophilicity in NPVs as compared to pure CGA. The amount of CGA found in water and n-octanol phase was 4.414 ± 0.026 mg/mL and 0.160 ± 0.060 mg/mL, respectively, with partition coefficient and Log P value of 0.036 ± 0.021 and − 1.44, respectively. While amount of CGA obtained in n-octanol phase of CGA 90H NPVs and CGA S100 NPVs was 4.580 ± 0.037 mg/mL (28.62 times) and 4.331 ± 0.023 mg/mL (26.81 times) higher than pure CGA ($P < 0.05$). Similar increasing amounts of CGA were obtained in water phase with 4.690 ± 0.108 mg/mL (1.05 times) of CGA 90H NPVs and 4.573 ± 0.038 mg/mL (1.02 times) of CGA S100 NPVs ($P < 0.05$). The mean particle size for CGA 90H NPVs and CGA S100 NPVs was 437.6 ± 31 nm and 449.6 ± 24.9 nm with PDI values 0.436 and 0.489,

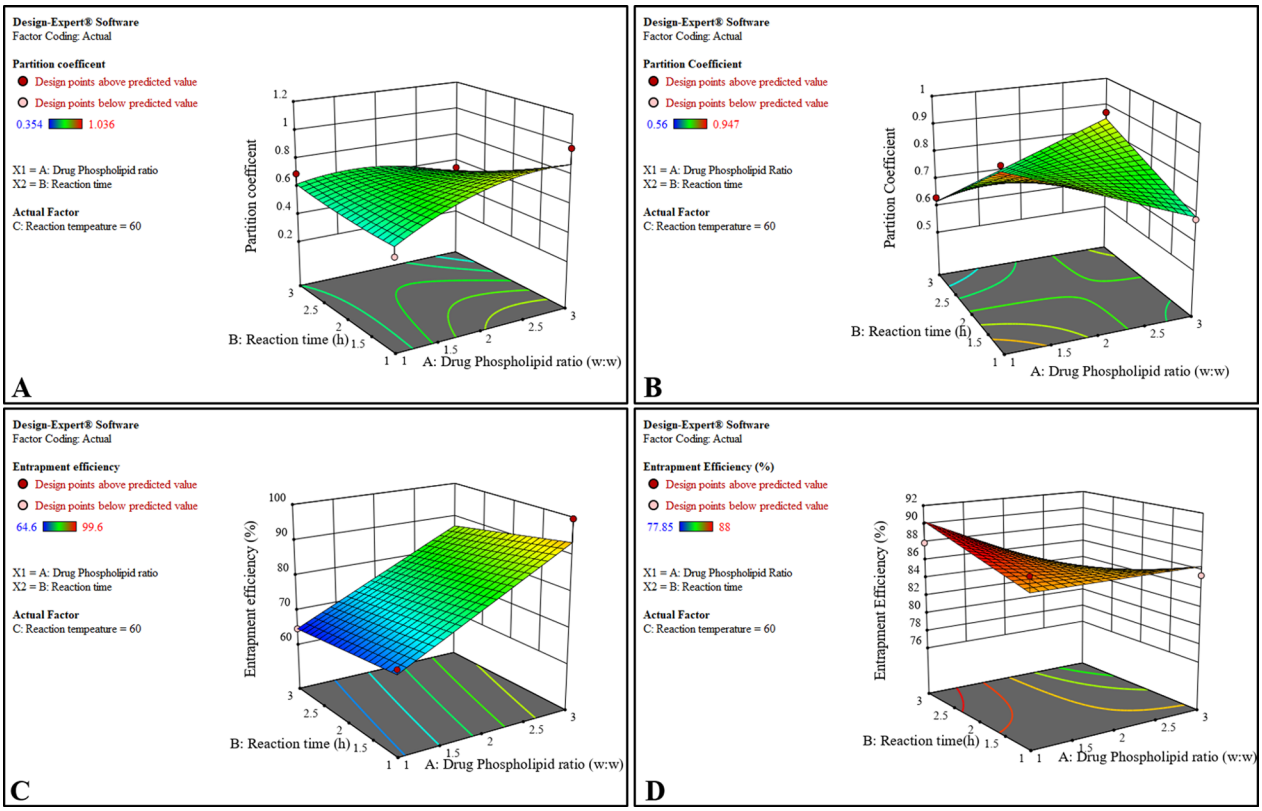

Fig. 1 3D surface plots showing the effects of independent variables (X_1: Drug phospholipid ratio, X_2: Reaction time, X_3: Reaction temperature) on **A** partition coefficient of CGA 90H NPVs, **B** partition coefficient of CGA S100 NPVs, **C** entrapment efficiency of CGA 90H NPVs and **D** entrapment efficiency of CGA S100 NPVs, respectively

respectively. PDI values < 0.5 indicate acceptable monodispersity and homogeneity in NPVs [48]. Zeta potential (-25.6 ± 4.39 mV and 29.3 ± 4.93 mV, respectively) results were in accordance with particle size range and close to -30 mV and + 30 mV showing stability [49]. TEM microscopy reiterated similar results showing a pentagonal and triangular structure of both CGA 90H NPVs and CGA S100 NPVs (Fig. 3A & B, respectively).

Fourier transform infrared spectroscopy (FTIR)

FTIR spectrums of pure CGA (A), both phospholipids (Phospholipon® 90H /Lipoid® S100) (B & C), their physical mixtures (D & E) and CGA NPVs, are shown in Fig. 4. Pure CGA showed characteristic phenolic OH group (3647 cm^{-1}) which broadened with CGA 90H NPVs (F) (3564.5–3901.99 cm^{-1}) and CGA S100 NPVs (G) (3670.54 cm^{-1}) [50]. Additionally, P = O stretch of Phospholipon® 90H (1467.83 cm^{-1}) and Lipoid® S100 (1080.14 cm^{-1}) shifted to lower wave number in CGA 90H NPVs (1417.12 cm^{-1}) with complete disappearance in CGA S100 NPVs. Also, the absence of N[CH_3] group and aromatic stretch peaks highlights the possible hydrogen bonding between N[CH_3] and OH group of CGA [17]. The FTIR spectra of physical mixtures retained all the characteristics of CGA and phospholipids (Phospholipon® 90H /Lipoid® S100), i.e. 970.19 cm^{-1} (N[CH_3] stretch); 3321.42–3849.92 cm^{-1} (phenolic OH stretch); 1658.79–1732.08 cm^{-1} (C = O stretch); 1456.26–1487.12 cm^{-1} (C–C = C stretch); 1506.41–1697.36 cm^{-1} (CH_2(C–H stretch) and 1465.9 cm^{-1} (P = O stretch) indicating CGA and phospholipids compatibility [28].

Differential scanning calorimetry (DSC)

CGA thermogram gave sharp endothermic peaks (A) (206.7 °C and 199.02 °C), which were consistent with earlier published reports [51]. While somewhat diffused endothermic peaks were obtained with Phospholipon® 90H (B) and Lipoid® S100 (C), indicating that as the temperature increased, the polar fractions of phospholipids melted (Fig. 5). This transition in physical state was due to the modification in hydrogen–carbon groups present [52]. Retention of characteristic peaks along with new peaks (75.18 °C and 128.09 °C with Phospholipon® 90H and Lipoid® S100, respectively) in the physical mixtures (D &E) was found. These new peaks can be attributed to depression in melting endotherm of partial phospholipid

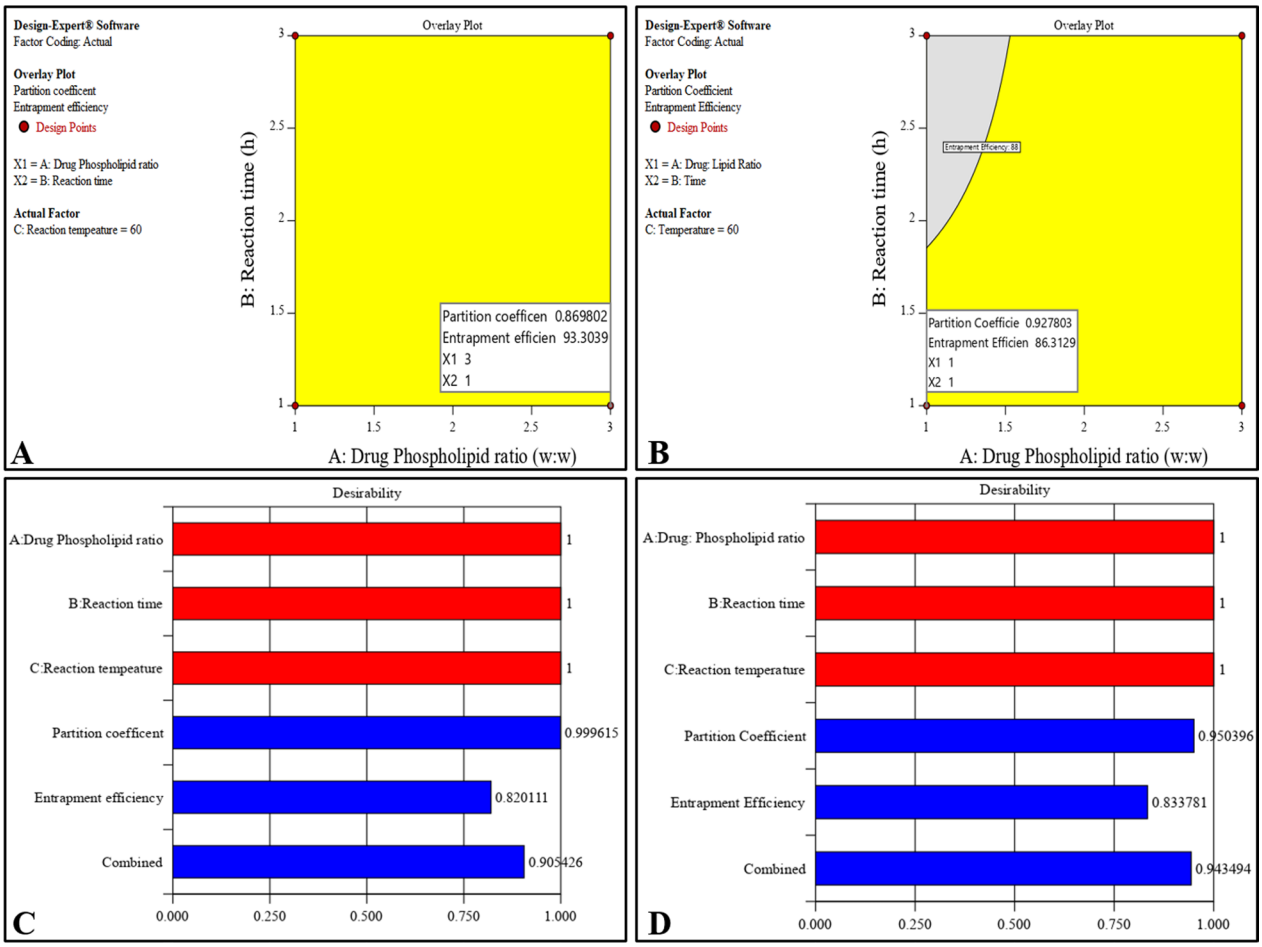

Fig. 2 Overlay plot for the validity of the design model exhibiting the predicted values for CGA 90H NPVs (**A**) and CGA S100 NPVs (**B**), respectively; Individual and combined desirability for measured responses for CGA 90H NPVs (**C**) and CGA S100 NPVs (**D**), respectively

Table 2 Predicted and observed values for the check point formulation analysis with CGA 90 H NPVs and CGA S100 NPVs

Formulation	Response	Predicted values	Observed values*	(%) Bias
CGA 90H NPVs	Partition coefficient	0.869	0.881 ± 0.48	− 1.38
	Entrapment efficiency (%)	93.3	95.7 ± 0.56	− 2.57
CGA S100 NPVs	Partition coefficient	0.927	0.942 ± 0.29	− 1.61
	Entrapment efficiency (%)	86.31	88.5 ± 0.66	− 2.53

* Data were represented as mean ± SD ($n = 3$)

adduct or formation of eutectic mixtures. While there was complete disappearance of excipient peaks in CGA 90H NPVs (F) (68.90 °C and 73.55 °C) and CGA S100 NPVs (G) (294.19 °C) indicating successful formulation [22].

High-performance thin-layer chromatography (HPTLC)

The Rf values obtained with pure CGA were 0.33 (peak 6 with 5µL (A)) and 0.35 (peak 3 &4 with 10 µL (B)) which corroborates with earlier published reports [53] (Fig. 6). An increase in Rf values was obtained for CGA 90H NPVs (peak 6 & 7 with 10 µL (D)) and CGA S100 NPVs (peak 4 with 5µL (E)) indicating non-polarity [54]. Increase in lipophilicity gave an indication of successful NPV formulation. While some peaks gave lower Rf values in CGA 90H NPVs (peak 2 with 5µL (C)) and CGA S100 NPVs (peak 2 with 10 µL (F)). This may be due to usage of non-polar solvent as mobile phase, which did not separate CGA (highly polar) at these particular concentrations.

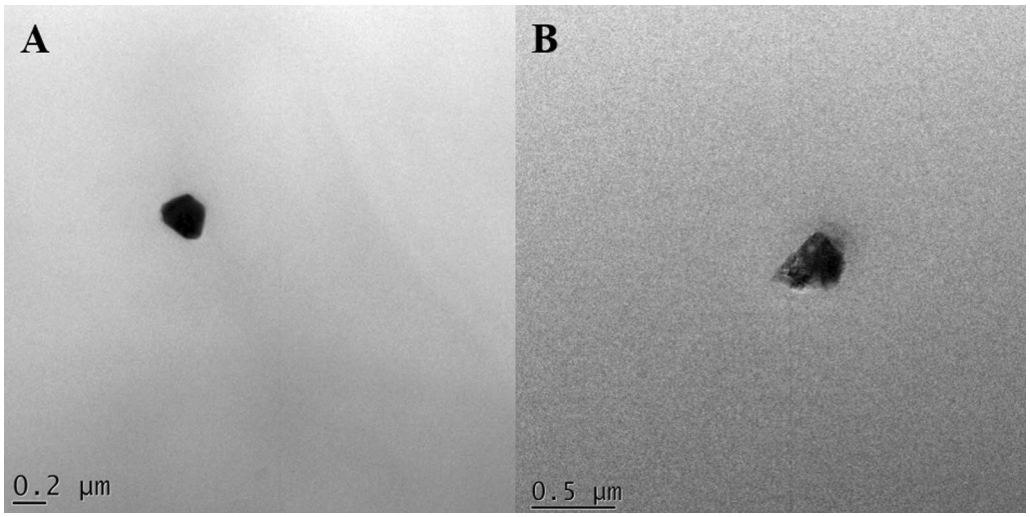

Fig. 3 Transmission electron microscopic images of CGA 90H NPVs (**A**) and CGA S100 NPVs (**B**)

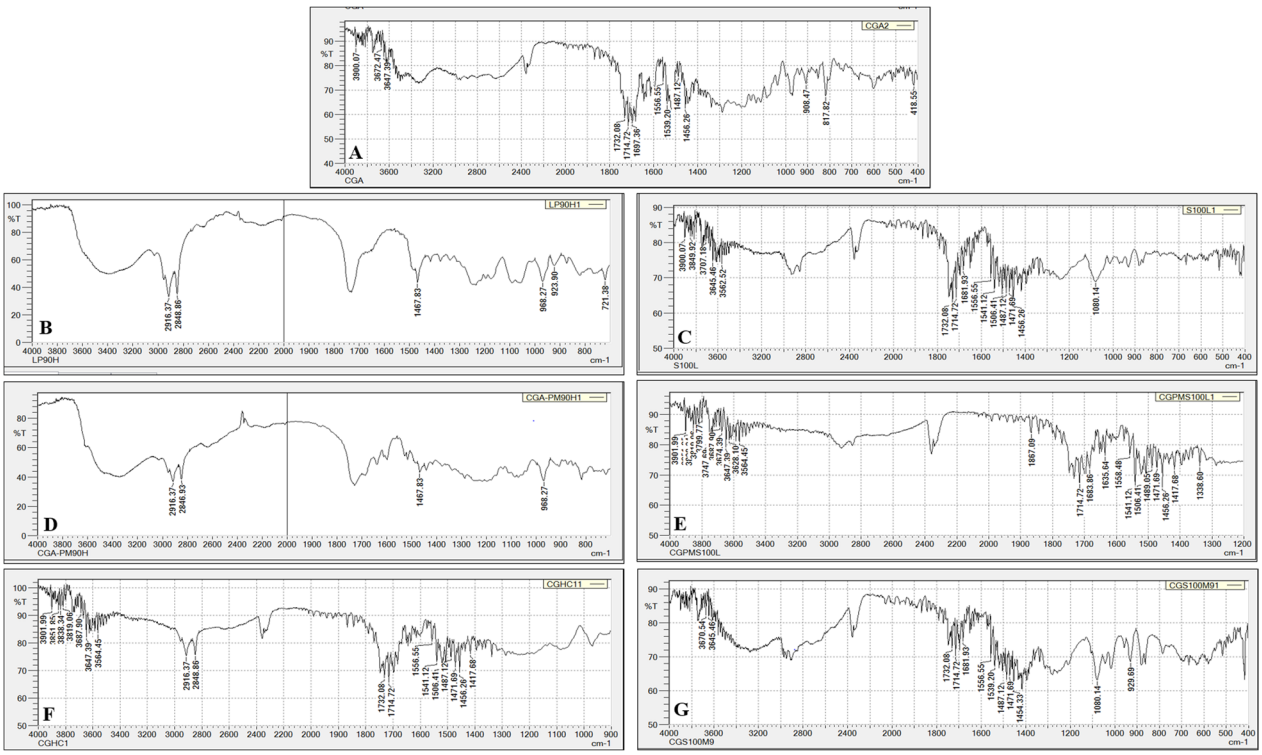

Fig. 4 FTIR spectra of **A** pure CGA, **B** Phospholipon® 90H, **C** Lipoid® S100, **D** Physical mixture of CGA: Phospholipon® 90H (1:1), **E** Physical mixture of CGA: Lipoid® S100 (1:1), **F** CGA 90H NPVs and **G** CGA S100 NPVs

[1]H-NMR analysis

The [1]H-NMR spectra of pure CGA and CGA NPVs formulations are shown in Fig. 7(A-C-E, respectively). Pure CGA [1]H-NMR spectrum (Fig. 7A) measured in d6-DMSO represents the phenyl protons in quinic-caffeic acid skeleton with peaks at the δ (ppm) 1.03 (1H, d, H-8) and 2.09 (1H, t, H-6). While the [1]H-NMR spectra of Phospholipon® 90H (Fig. 7B) and Lipoid® S100 (Fig. 7D) showed characteristic aliphatic side chain hydrogens at δ 55.99 (s, H-23) and δ 34.59 (d, H-15). Compared to the

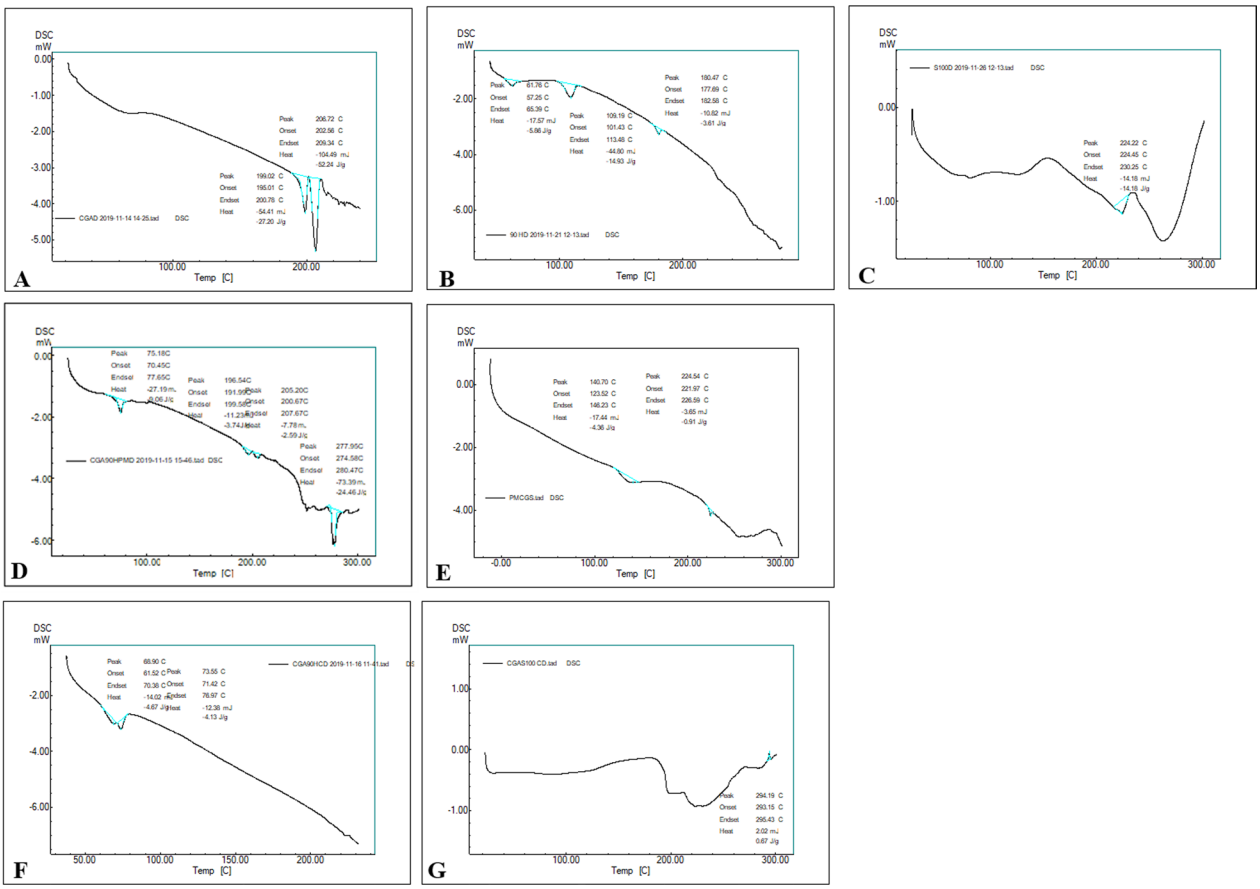

Fig. 5 DSC thermograms of **A** pure CGA, **B** Phospholipon® 90H, **C** Lipoid® S100, **D** Physical mixture of CGA: Phospholipon® 90H (1:1), **E** Physical mixture of CGA: Lipoid® S100 (1:1), **F** CGA 90H NPVs and **G** CGA S100 NPVs

CGA and phospholipids, peak obtained with CGA 90H NPVs (C) and CGA S100 NPVs (E) showed lower intensity and broader signals (δ 26.06 (s, H-8) and δ 20.14 (d, H-2), respectively). Also, disappearance of distinct CGA peaks at δ 0.72 (1H, s, OH-5) and 1.01 (1H, s, OH-4) from CGA 90H NPVs and CGA S100 NPVs indicated intermolecular bonding between phenolic OH groups with polar groups of both the phospholipids (Fig. 7C and E) [55].

In vitro dissolution studies

A comparative dissolution behaviour for CGA, CGA 90H NPVs and CGA S100 NPVs is demonstrated in Fig. 8A. CGA gave the highest cumulative release within the first 8 h (89.8 ± 1.39) as compared to (44.7 ± 0.26) of CGA 90H NPVs and (43.6 ± 1.05) of CGA S100 NPVs. The final per cent cumulative drug release at 24 h was (90.4 ± 0.48%) of CGA in comparison with a more sustained drug release of CGA 90H NPVs (98.36 ± 1.02%) and CGA S100 NPVs (94.87 ± 1.34%) ($< P = 0.001$). The release data were also analysed using mathematical kinetic models which showed that the drug release mechanism followed by CGA was quasi-Fickian ($n < 0.45$) and followed Korsmeyer–Peppas model ($R^2 = 0.991$, $n = 0.06$) exhibiting relaxed controlled diffusion, while CGA 90H NPVs and CGA S100 NPVs followed Higuchi model ($R^2 = 0.981$, $n = 0.32$ and $R^2 = 0.974$, $n = 0.37$, respectively) exhibiting dissociation and diffusion mechanism [33].

Evaluation of NPVs hydrogel formulation

Optimum viscosity of 11,290 ± 2.4cps, 11,350 ± 1.6cps and 23,900 ± 1.4cps was obtained with 1% CGA hydrogel, CGA 90 NPVs and CGA S100 NPVs hydrogels at minimum shear rates ($P > 0.05$). CGA S100 NPVs hydrogel displayed more viscosity because of the high phosphatidylcholine content of LIPOID® S100 making it comparatively less spreadable [56]. Maximum drug content values were obtained with all the three hydrogels (97.31 ± 0.25%, 98.54 ± 0.41% and 98.01 ± 0.87%, respectively ($P < 0.05$) with pH close to the skin pH showing compatibility and stability. While the Draize patch test revealed that negative control (Group I(A)) showed no oedema as compared to the positive control (B) with erythema and

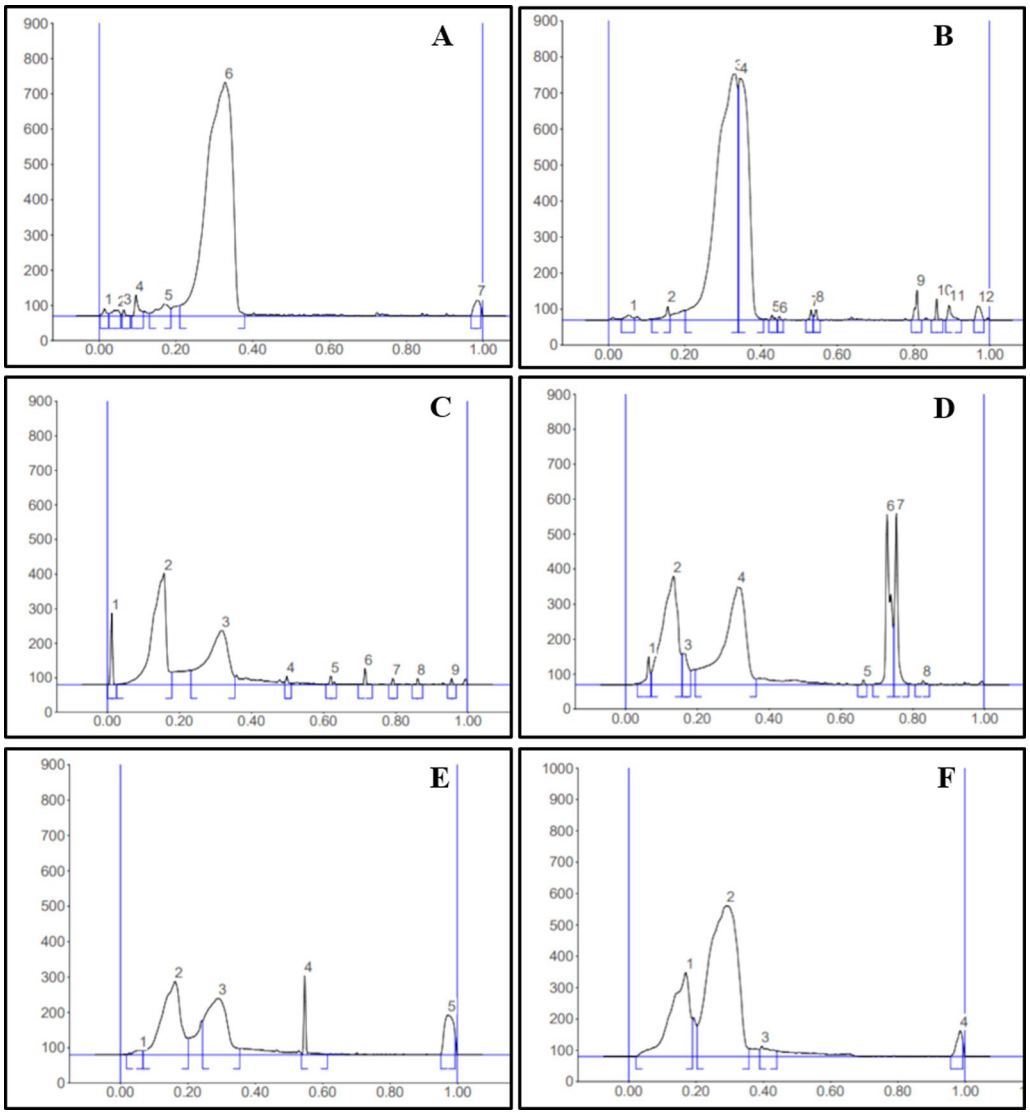

Fig. 6 HPTLC chromatograms at 5 µL and 10 µL of CGA (**A**&**B**), CGA 90H NPVs (**C**&**D**) and CGA S100 NPVs (**E**&**F**)

oedema of higher degree (Fig. 9). Group III(C), IV(D) and V(E) were free of any irritation or oedema highlighting the safety of the topical Carbopol hydrogels even after prolonged periods of application [57]

Drug diffusion and permeation data

In vitro drug diffusion profile of CGA, CGA 90H NPVs and CGA S100 NPVs hydrogels are illustrated in Fig. 8B revealing a sustained diffusion of CGA from CGA90H NPVs hydrogel (101.9 ± 1.12%) and CGA S100 NPVs hydrogel (99.9 ± 1.64%) for a period of 48 h as compared to CGA hydrogel (88.1 ± 1.32%) ($< P = 0.001$). The release data of all the three hydrogels were studied with different kinetic models. Following analysis, it was found that CGA 90H NPVs hydrogel and CGA hydrogel followed Korsmeyer–Peppas model ($R^2 = 0.971$ and $R^2 = 0.883$, respectively) with exponent value of $n = 0.55$ & $n = 0.36$, thus exhibiting non-Fickian diffusion through polymeric matrix system for CGA 90H NPVs hydrogel and relaxed controlled diffusion for CGA hydrogel. While CGA S100 NPVs hydrogel followed first-order model ($R^2 = 0.969$; $n = 0.6$) indicating drug diffusion through swellable matrix of non-Fickian diffusion.

A significant increase in permeability of CGA 90H NPVs and CGA S100 NPVs hydrogels over CGA hydrogel was obtained ($< P = 0.001$). The per cent cumulative CGA permeated (Eq. 10) over the period of 48 h from CGA 90H NPVs and CGA S100 NPVs hydrogels was

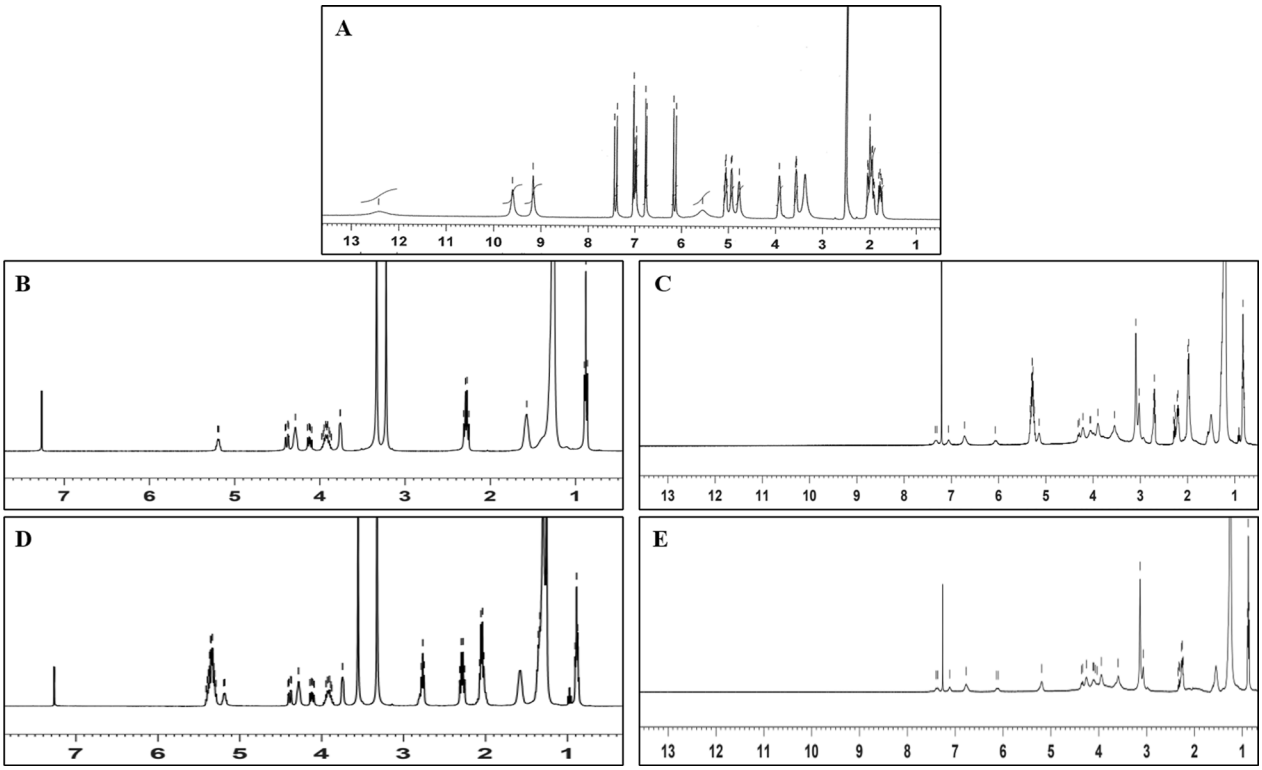

Fig. 7 ^{1}H NMR spectra of **A** pure CGA, **B** Phospholipon® 90H, **D** Lipoid® S100, **C** CGA 90H NPVs and **E** CGA S100 NPVs

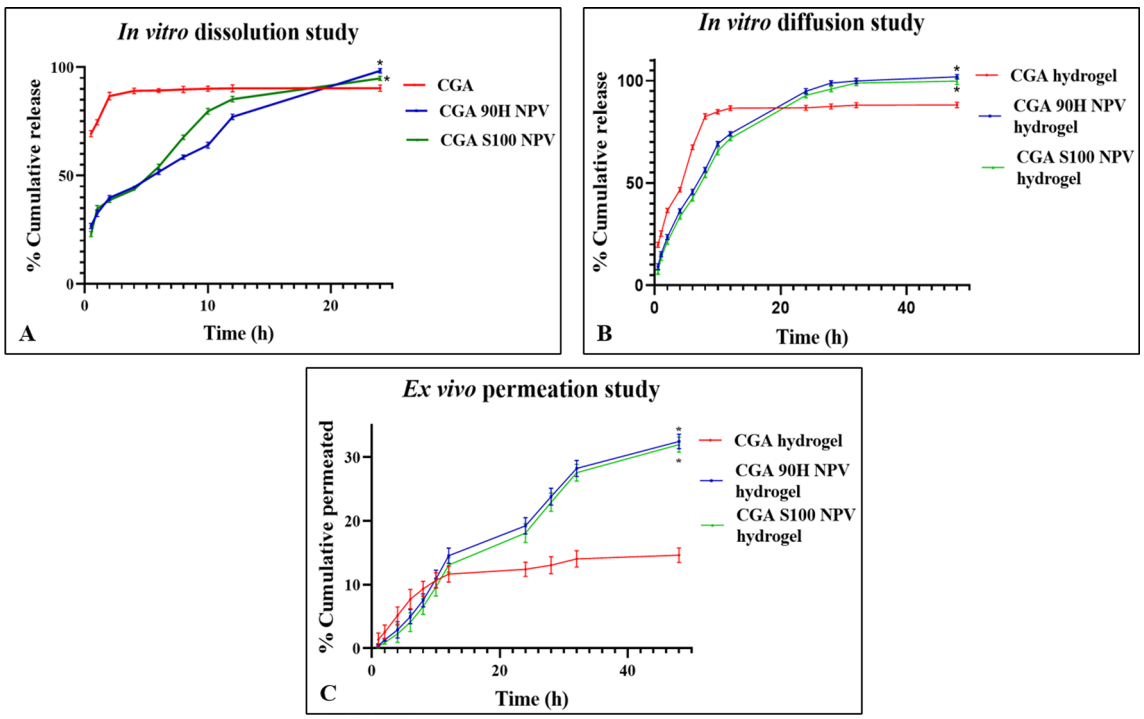

Fig. 8 In vitro dissolution profile **A** of CGA release from CGA 90H NPVs suspension and CGA S100 NPVs suspension.; In vitro diffusion profile **B** of CGA release from CGA 90H NPVs hydrogel and CGA S100 NPVs hydrogel; Ex vivo permeability profile **C** of CGA, CGA 90H NPVs hydrogel and CGA S100 NPVs hydrogel. Values are mean ± Std. Dev. ($n = 3$); * $P < 0.001$ significant with respect to CGA

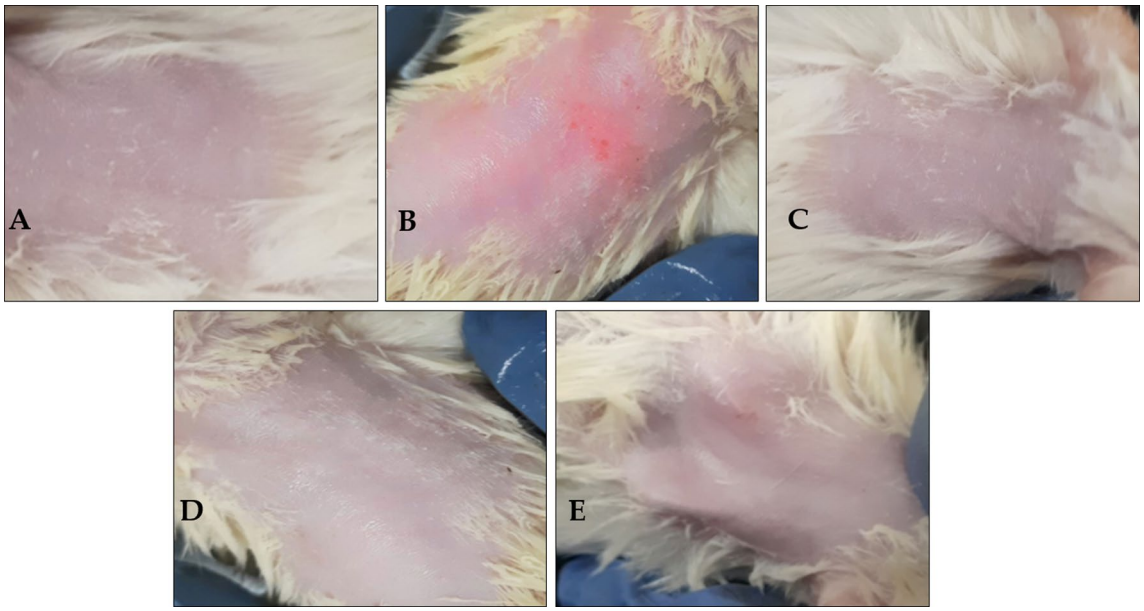

Fig. 9 Examination of skin irritancy. **A** Group I receiving blank hydrogel, **B** Group II receiving 0.8%v/v formalin showing oedema and erythema with **C** Group III 1% CGA hydrogel, **D** Group IV CGA 90H NPVs hydrogel (E) Group V CGA S100 NPVs hydrogel showing no redness or oedema

Table 3 Comparative permeation ability of CGA 90H NPVs, CGA S100 NPVs hydrogel against CGA hydrogel

Formulation	Steady state flux *Jss* (µg/cm^2/h)	Permeability coefficient (cm/h)	Enhancement ratio of flux
CGA hydrogel	22.58 ± 1.087	49X10^{-3} ± 2.16	–
CGA 90H NPVs hydrogel	25.23 ± 1.66	63X10^{-3} ± 1.89	1.11 ± 0.57*
CGA S100 NPVs hydrogel	23.86 ± 1.91	59 X10^{-3} ± 2.21	1.05 ± 0.43*

Data were represented as mean ± SD ($n = 3$)

* $P < 0.001$ compared with CGA hydrogel

(32.49 ± 1.16%) 2.22 times and (31.98 ± 1.21%) 2.19 times higher (respectively) than CGA hydrogel (14.63 ± 1.15%) (Fig. 8C). Other permeation parameters like steady-state flux, permeability coefficient and enhancement in flux ratio (Table 3) also showed values 1.11 ± 0.57 times and 1.05 ± 0.43 times higher with CGA 90H NPVs and CGA S100 NPVs hydrogels than CGA hydrogel ($< P = 0.001$).

The permeation ability of CGA 90H NPVs and CGA S100 NPV hydrogels to reach deeper layers of skin was further affirmed by CLSM study by tagging 0.03% of RHO 6G in standard and test samples. The CLSM images of CGA 90H NPVs RHO hydrogel and CGA S100 RHO NPVs hydrogel along with CGA RHO hydrogel (standard) are shown in Fig. 10. It was observed that CGA RHO hydrogel (A)(standard) showed lower fluorescence intensity restricted to the shallow layers of skin as comparison to CGA 90H NPVs RHO hydrogel (B) and CGA S100 RHO NPVs hydrogel (C) [35], which showed higher intensity of fluorescence distributed evenly through the entire skin tissue.

Stability studies

Extensive study has been carried out to determine the stability of phenolic derivatives like CGA. Narita et al. studied the degradation kinetics of CGA and other derivatives of 5-caffeoylquinic acid at higher temperatures and pH with respect to time [15]. While some research groups demonstrated the negative effect of storage and processing on CGA [58, 59]. This was in contrast to the stability obtained with optimized CGA 90H NPVs and CGA S100 NPVs assessed by measuring partition coefficient, entrapment efficiency and zeta potential values for 6-month period at 25 °C ± 2 °C/60% RH ± 5% RH & 2–8 °C. No significant changes were observed over this period indicating the stable nature of both the NPVs (Table 4). Similarly, formulated hydrogel preparations were found to be stable at refrigerated conditions with no significant changes in pH or drug content values over the period of 3 months.

In vitro antioxidant and cell viability study

The antioxidant potential of CGA 90H NPVs and CGA S100 NPVs was determined and compared with pure CGA by two different assay techniques. Higher Fe^{2+} chelation ability was seen with CGA 90H NPVs (80.36 ± 0.19%) and CGA S100 NPVs (78.12 ± 0.86%) as compared to CGA (82.72 ± 0.62%) ($< P = 0.001$) (Fig. 11B).

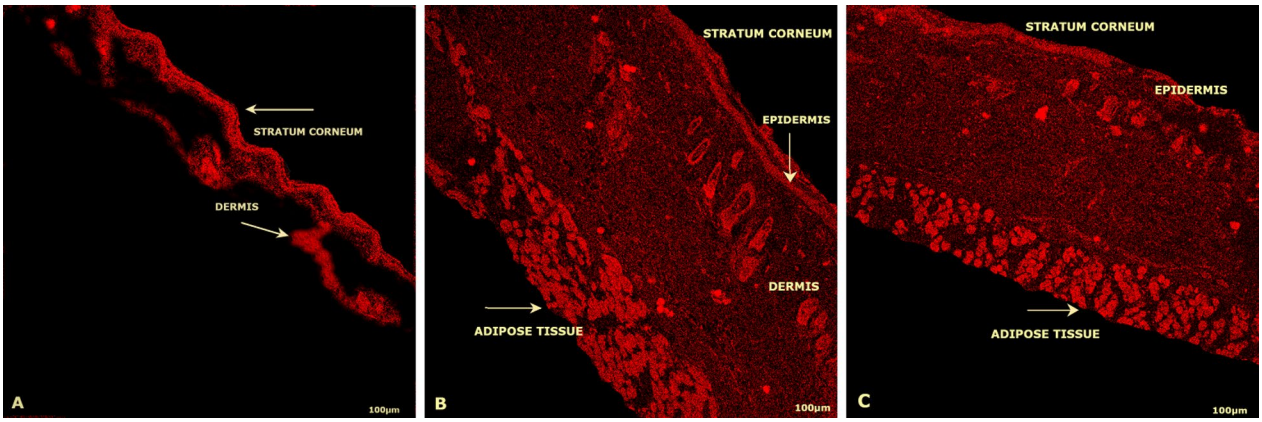

Fig. 10 Confocal microscopic images. **A** CGA RHO hydrogel showing low-intensity fluorescence in shallow layers of epidermis as compared to **B** CGA 90H NPVs RHO hydrogel and **C** CGA S100 NPVs RHO hydrogel showing evenly distributed fluorescence throughout the rat skin tissue

Table 4 Stability profile of CGA 90H NPVs and CGA S100 NPVs

Storage conditions	Time interval	CGA 90H NPVs			CGA S100 NPVs		
	(Months)	EE (%)	PC	ZP(mV)	EE (%)	PC	ZP (mV)
25 °C ± 2 °C/60%RH ± 5%RH	0	99.60 ± 0.17	0.977 ± 0.5	− 25.6	87.89 ± 0.68	0.947 ± 0.0	− 29.3
	3	98.15 ± 0.07	0.976 ± 0.2	− 25.1	86.96 ± 0.19	0.946 ± 0.7	− 28.9
	6	97.83 ± 0.02	0.975 ± 0.5	− 24.7	86.43 ± 0.01	0.945 ± 0.8	− 28.2
5 °C ± 3 °C	0	99.60 ± 0.17	0.977 ± 0.5	− 25.6	87.89 ± 0.68	0.947 ± 0.0	− 29.3
	3	99.03 ± 0.09	0.977 ± 0.9	− 25.2	87.56 ± 0.08	0.947 ± 0.4	− 29.1
	6	98.83 ± 0.10	0.976 ± 0.0	− 24.9	87.06 ± 0.01	0.946 ± 0.8	− 28.8

Data were represented as mean ± SD ($n = 3$)

EE Entrapment efficiency, *PC* Partition coefficient, *ZP* Zeta potential

Similar observation was made with DPPH radical scavenging assay which depicted higher radical scavenging activity of CGA 90H NPVs (96.74 ± 0.09%) and CGA S100 NPVs (95.12 ± 0.86%) as compared to CGA (83.79 ± 0.62%) ($< P = 0.001$), thus exhibiting the efficiency of the NPV formulation (Fig. 11A).

The cell viability in HeLa cells decreased from (107.7 ± 1.16% to 0.2 ± 0.08%) and (105.5 ± 1.04% to 0.1 ± 0.07%) for CGA 90H NPVs and CGA S100 NPVs as compared to (101.1 ± 1.28% to 1.2 ± 1.07%) for pure CGA ($< P = 0.001$) with increasing concentration of CGA from 0.2 to 3.4 mg/mL (Fig. 11C). Similar manner of dose-dependent decrease in cell viability was seen in HL-60 cells (Fig. 11D) with per cent cell viability decreasing from 100.6 ± 1.54% to 1.7 ± 0.82%; 106.5 ± 0.29% to 1.5 ± 0.66% and 108.8 ± 1.21% to 1.8 ± 0.71% for CGA, CGA 90H NPVs and CGA S100 NPVs, respectively ($< P = 0.001$). Furthermore, the IC_{50} values calculated from the per cent cell viability data as the concentration required to inhibit 50% of HeLa or HL-60 cells was found to be lower for CGA NPVs (0.75 times lower with CGA S100 NPVs in HeLa cells and 0.75 times lower with CGA 90H NPVs in HL-60 cells) as compared to pure CGA (Table 5), thus exhibiting the efficiency of NPV formulation. The survival inhibition of HeLa and HL-60 cells with increased concentration of CGA NPVs confirmed the anticancer activity and proved the potential of CGA NPVs in cervical and leukaemia cancer.

Pharmacodynamic study: wound-healing activity

The wound area was measured and captured (Fig. 12) for a period of 15 days, which showed completed closure of wound at 12th day with CGA 90H NPVs and CGA S100 NPVs hydrogel as compared to CGA hydrogel and marketed Silverex® heal hydrogel. Similar results were obtained with wound contraction percentage of CGA 90H NPVs and CGA S100 NPVs hydrogel, which were significantly higher than CGA hydrogel and marketed Silverex® heal hydrogel (Table 6). Statistical analysis

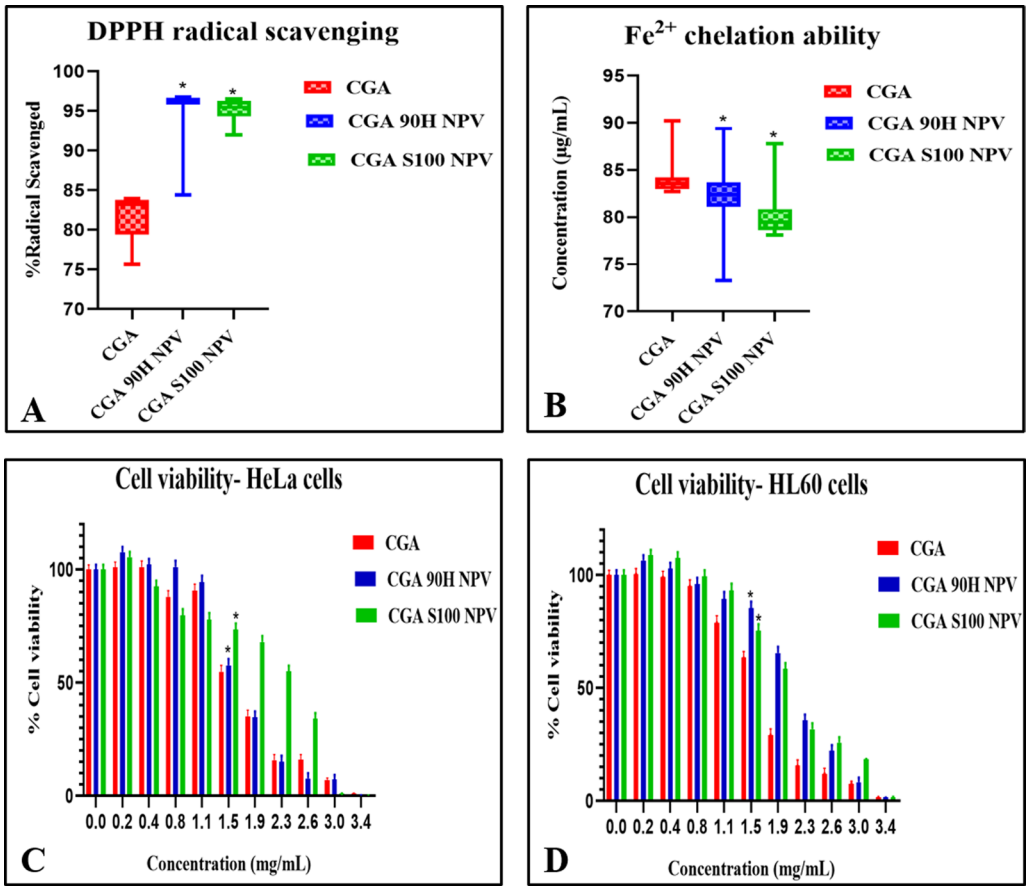

Fig. 11 Antioxidant studies **A** comparative DPPH radical scavenging activity and **B** Fe^{2+} chelation ability of CGA, CGA 90H NPVs and CGA S100 NPVs, MTT cell viability assay of CGA, CGA 90H NPVs and CGA S100 NPVs on HeLa cells (**C**) and HL-60 cells (**D**). Values are mean ± Std. Dev. ($n = 3$); * $P < 0.001$ significant with respect to CGA

Table 5 IC_{50} values for CGA, CGA 90H NPVs and CGA S100 NPVs on HeLa and HL-60 cells

Calculated IC_{50} (µg/ml)					
HeLa			HL-60		
CGA	CGA 90H NPVs	CGA S100 NPVs	CGA	CGA 90H NPVs	CGA S100 NPVs
1.36 ± 0.2	1.30 ± 0.14*	1.02 ± 0.16*	1.18 ± 0.82	0.88 ± 0.18*	0.99 ± 0.13*

Data were represented as mean ± SD ($n = 3$)

* $P < 0.001$ compared with CGA

carried out with GraphPad Prism 8.0.2 using ANOVA and Student's t test gave significant P values ($< P = 0.05$ and $P < 0.01$). It was found that CGA S100 NPVs hydrogel was more efficacious with higher reduction in wound area (50.26 ± 3.4 mm) and percentage of wound contraction values (71.56%) at day 3 itself than CGA 90H NPVs hydrogel (132.7 ± 2.5 mm and 34.0%) ($P < 0.05$). This was in contraction to ex vivo permeation results which showed lower flux values for CGA S100 NPVs hydrogel as compared to CGA 90H NPVs hydrogel.

These results were reiterated with histopathological study of skin specimens, which gave more insight on the healing phase (Fig. 13). Day 6 skin specimens showed irregular skin structures with the absence of epithelial layer with CGA hydrogel. Similar irregular stratum spinosum and stratum granulosum layers were seen with CGA NPVs hydrogel. In comparison with day 6, day 12 skin sections showed larger number of fibroblasts with thick collagen fibres and complete epithelization with CGA S100 NPV and CGA90H NPV hydrogel. However, CGA hydrogel skin section still showed incomplete epithelization on day 12 [60].

Pharmacokinetic study: oral bioavailability studies

Oral bioavailability, i.e. mean plasma concentration time profiles of pure CGA (group II; 100 mg/kg oral) and CGA NPVs (Group III and IV; ~ 100 mg/kg oral), is given in Fig. 14A. Significant increases in

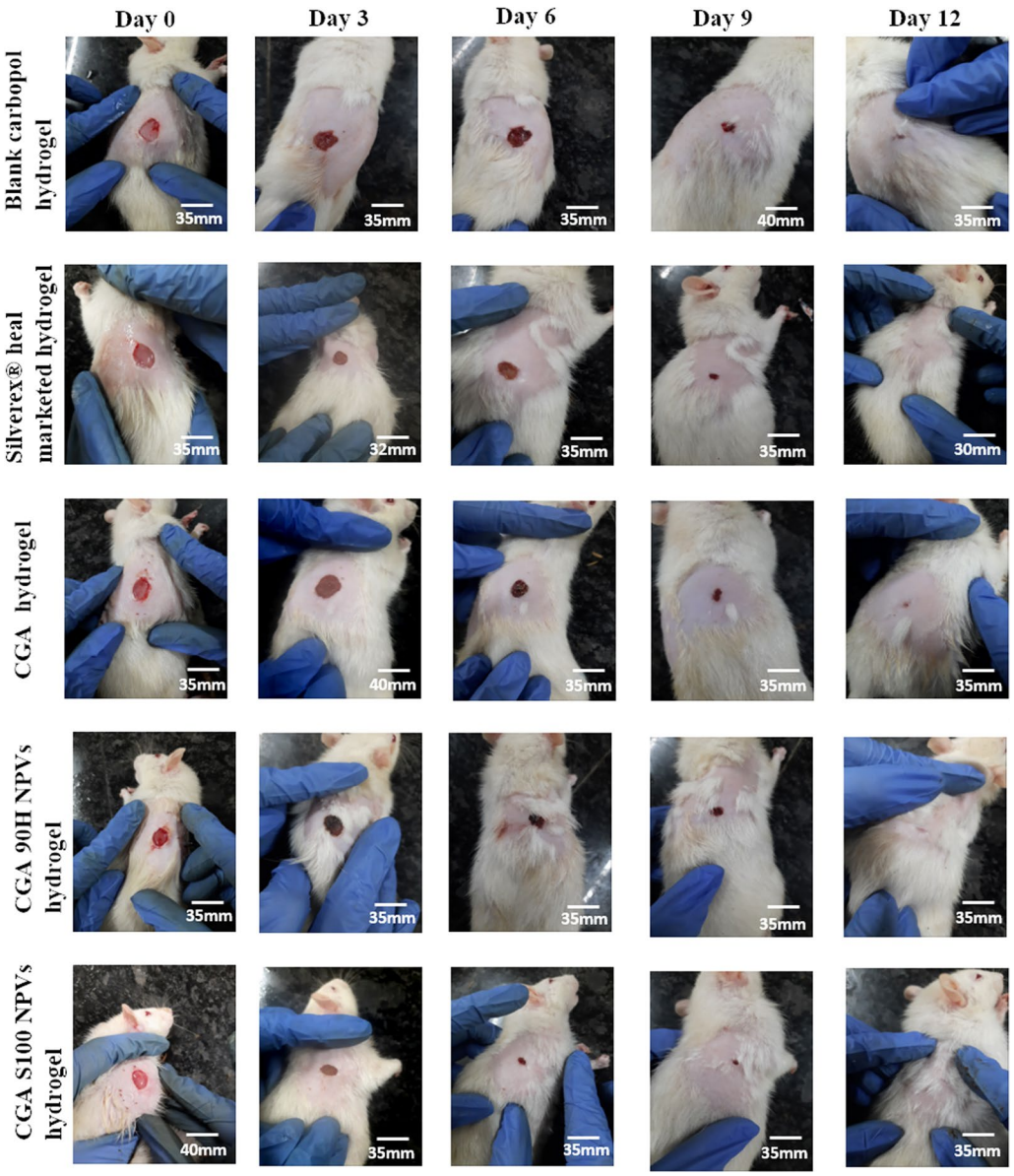

Fig. 12 Images of full thickness skin excision on dorsal thoracic surface of rats. Wounds were treated once daily with respective hydrogels and were photographed on days 0, 3, 6, 9 and 12th day with CGA 90H NPVs and CGA S100 NPVs hydrogel showing complete re-epithelization and regrowth of dorsal hair at 12th day in comparison with CGA hydrogel and Silverex® heal marketed hydrogel showing incomplete epithelization

the plasma concentration time profiles were obtained with both NPVs (CG 90H NPV and CGA S100 NPV) up to 8 h as compared to pure CGA. CGA gave highest C_{max} (~41.9 ± 1.78 µg/mL) at ~0.5 h with linear decrease in plasma concentration thereafter till 8 h (5.0 ± 1.11 µg/mL). While CGA 90H NPVs gave highest $C_{\max}$ (~47.5 ± 1.11 µg/mL) at ~1 h with a sustained mean plasma concentration till 8 h with ~39.1 ± 1.88 µg/mL. CGA S100 NPVs gave (lower $C_{\max}$ values than CGA 90H NPV) highest $C_{\max}$ ~31.7 ± 1.23 µg/mL at ~0.5 h with sustain mean plasma concentration of ~20.7 ± 1.29 µg/mL till ~8 h ($P < 0.005$). This sustained effect of CGA 90H NPVs and CGA S100 NPVs was in accordance with the dissolution and diffusion data. Statistical software (PK solver) further estimated additional pharmacokinetic parameters (Table 7) expressing relative bioavailability such as *Cmax, Tmax and* $AUC_{0\text{-}t}$ which were significantly higher in group treated with NPVs as to the group receiving pure CGA. CGA NPVs significantly enhanced AUC $_{0\text{-}t}$ value (~327.23 µg/mL*h and ~183.85 µg/mL*h, respectively) compared to lower AUC $_{0\text{-}t}$ value of pure CGA (~110.43 µg/mL*h) indicating the higher oral

Table 6 Wound contraction area and per cent wound contraction values for CGA and CGA NPVs hydrogels

Post-wounding (Days)	Blank carbopol hydrogel*	Marketed hydrogel (Silverex® heal)*	CGA hydrogel*	CGA 90H NPVs hydrogel*	CGA S100 NPVs hydrogel*
0	196.70 ± 2.3	196.70 ± 3.6	198.70 ± 3.5	201.05 ± 2.8	196.70 ± 3.7
3	132.70 ± 2.9[c] (24.90%)	63.61 ± 4.1 [a,c] (64.0%)	113.09 ± 2.8[a] (36.0%)	132.7 ± 2.5 [a,c] (34.0%)	50.26 ± 3.4 [a,c] (71.56%)
6	95.03 ± 3.1[d] (46.22%)	28.27 ± 1.6 [b,c] (84.0%)	63.61 ± 1.9[b] (64.00%)	38.48 ± 3.1 [b,c] (80.86%)	19.63 ± 2.9 [b,d] (88.89%)
9	20.63 ± 1.9[d] (87.19%)	12.56 ± 2.4 [b,c] (92.89%)	19.43 ± 4.2[b] (88.89%)	3.14 ± 2.7 [b,c] (98.44%)	3.14 ± 3.1 [b,d] (98.62%)
12	3.14 ± 2.5[d] (98.22%)	0.78 ± 0.8 [b,d] (99.56%)	0.78 ± 0.4[b] (99.56%)	0.78 ± 0.23 [b,d] (99.61%)	0.78 ± 0.45 [b,d] (99.56%)
15	0.78 ± 0.5 [d] (99.56%)	∞	0.14 ± 0.02[b] (99.92%)	∞	∞

∞ Indicates that the wound was completely healed

* Data were represented as mean ± SD ($n = 5$)

[a] $P < 0.05$ and [b] $P < 0.01$, compared with blank Carbopol hydrogel

[c] $P < 0.05$ and [d] $P < 0.01$ compared to the values of CGA hydrogel

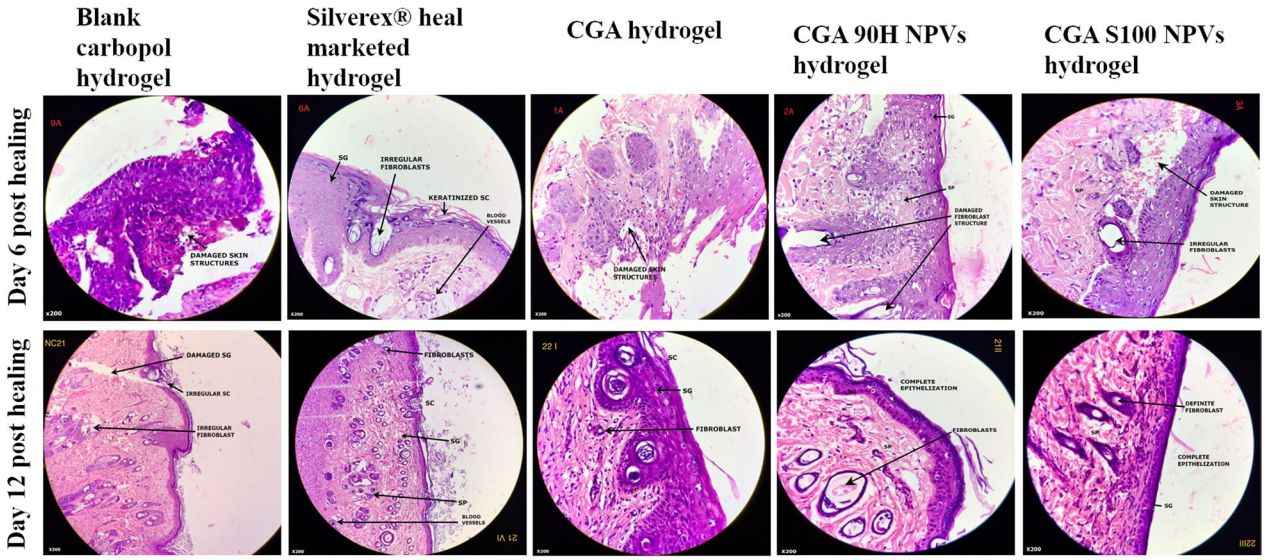

Fig. 13 Histopathological study of unhealed (Day 6) and healed wound (Day 12) skin sections stained with haematoxylin–eosin dye. The photomicrographs show sections treated with CGA 90H NPVs and CGA S100 NPVs hydrogel in comparison to 1% CGA hydrogel, Silverex® heal marketed hydrogel and blank hydrogel. Abbreviations: SC, Stratum corneum; SG, Stratum granulosum; SP, Stratum spinosum

bioavailability of NPVs. NPVs also improved the mean residence time (*MRT*) value (~ 37.75 h and ~ 32.64 h, respectively) compared to lower *MRT* value of CGA (~ 3.51 h) highlighting the availability of NPV in the body after oral administration. Furthermore, NPVs not only improved elimination half-life($t_{1/2}$) (25.87 h and 22.53 h of NPVs as compared to 2.36 h of pure CGA but also improved the clearance (*cl/F*) and volume of distribution (*Vz/F*). The computed bioavailability (F) of CGA after CGA 90H NPVs and CGA S100 NPVs administration was found to be 105.67% and 101.88%, respectively.

Additionally, correlation between the per cent drug released and per cent drug absorbed was determined using Wagner–Nelson equation. The values for in vitro release and in vivo absorbed over the period of 8 h is compared in Table 8 for CGA and CGA NPVs. The *IVIVC* showed that in vitro drug dissolution was rapid for pure CGA (0.5-1 h) which was in accordance with earlier reports stating that maximum drug release occurs within 0.5 h because of the low half-life of CGA [14]. On the other hand, a more sustained in vitro dissolution and in vivo absorption values were obtained with CGA 90H NPVs and CGA S100 NPVs($P < 0.005$). The overlayered plots of (Fig. 14C–D) CGA 90H NPVs and CGA S100 NPVs for in vitro drug release and in vivo absorption indicate correlation and thus can it can be

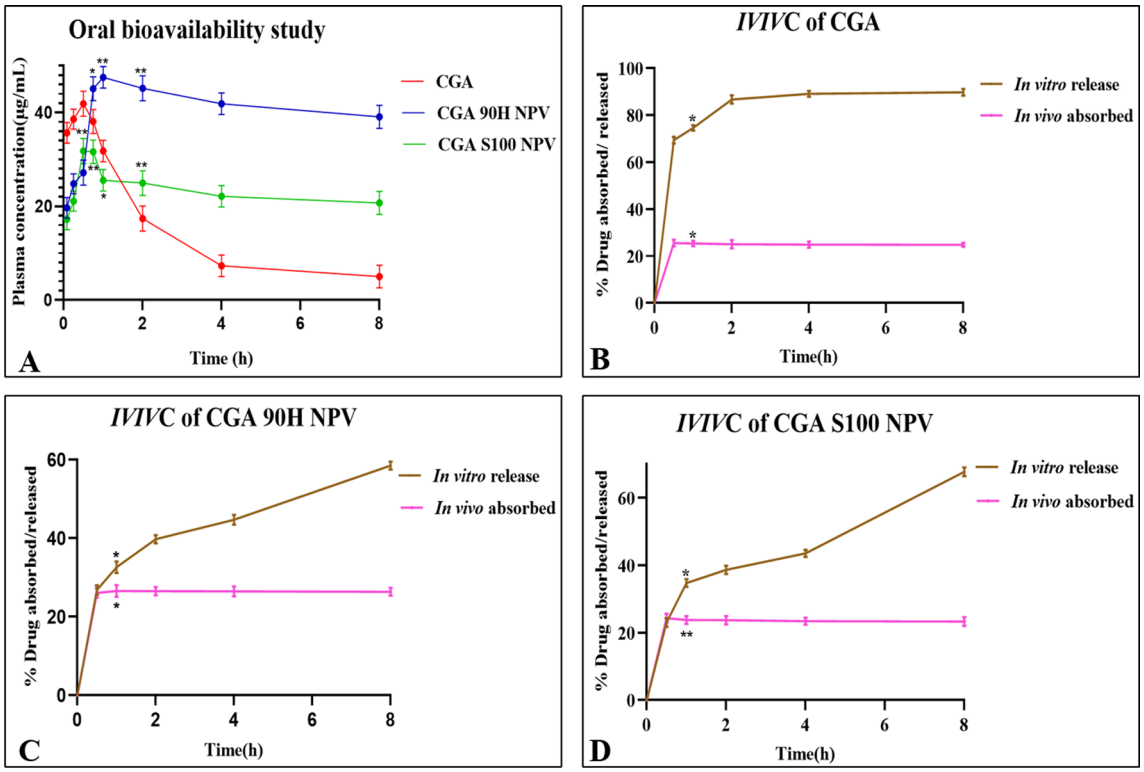

Fig. 14 Mean plasma concentration time profile after oral administration of CGA suspension (100 mg/kg) and CGA 90H NPV and CGA S100 NPV suspension (~ 100 mg/kg); in vitro in vivo correlation plots for CGA, CGA 90H NPVs and CGA S100 NPVs. Values are mean ± Std. Dev. ($n = 5$); * $P < 0.005$, ** $P < 0.001$ significant with respect to CGA

Table 7 Estimated pharmacokinetic parameters after oral administration of CGA and CGA NPVs

Pharmacokinetic parameters	CGA	CGA 90H NPVs	CGA S100 NPVs
C_{max} (µg/mL)	41.9 ± 1.78	47.5 ± 1.11	31.8 ± 1.56
T_{max} (h)	0.5	1	0.5
Elimination half-life ($t_{1/2}$) (h)	2.36	25.87	22.53
Elimination rate constant (K_{el})(h^{-1})	0.29	0.028	0.031
Area under concentration–time curve (AUC $_{0\text{-}t}$) (µg mL^{-1} h)	110.43	327.23	183.85
Area under concentration–time curve ($AUC_{0-\infty}$) (µg mL^{-1} h)	127.32	1786.97	858.08
Mean residence time (MRT)(h)	3.51	37.75	32.64
Clearance(*cl/F*) [(mg)/(µg/ml^{-1})/h^{-1}]	0.79	0.06	0.12
Volume of distribution (*Vz/F*) [(mg)/(µg/ml^{-1})]	2.68	2.09	3.79

Data were represented as mean ± SD ($n = 5$)

implied that in vitro dissolution studies served as a representative understudy for in vivo bioavailability study.

Discussion

CGA, despite its wild occurrence in nature and proven effective application in various pharmacotherapeutic conditions, is not utilized because of its poor physiochemical properties. This study is the first of its kind to improve all of its physicochemical properties like solubility, permeability, bioavailability, stability and examine efficiency in healing wounds along with antioxidant and anticancer potential. To achieve this, CGA 90H NPVs and CGA S100 NPVs were formulated and optimized using CCD. CCD scrutinized the best suitable experimental models supported by centre, axial and factorial points [61] of independent factors (drug phospholipid ratio, reaction time and reaction temperatures) measured by dependent factors (partition coefficient and entrapment efficiency).

Table 8 Comparative *IVIV*C data for CGA, CGA 90H NPVs and CGA S100 NPVs

Time (h)	CGA (%)		CGA 90H NPVs (%)		CGA S100 NPVs (%)	
	In vitro released	In vivo absorbed	In vitro released	In vivo absorbed	In vitro released	In vivo absorbed
0	0	0	0	0	0	0
0.5	69.4 ± 1.45	25.55 ± 1.05	26.8 ± 1.21	26.09 ± 1.22	23.0 ± 1.34	24.32 ± 1.05
1	74.6 ± 1.23	25.35 ± 1.53	32.6 ± 1.49	26.58 ± 1.07	34.7 ± 1.18	23.76 ± 1.11
2	86.7 ± 1.75	25.06 ± 1.28	39.8 ± 1.07	26.53 ± 1.37	38.7 ± 1.25	23.70 ± 1.28
4	89.1 ± 1.31	24.86 ± 1.19	44.7 ± 0.26	26.45 ± 1.41	43.6 ± 1.05	23.44 ± 1.16
8	89.8 ± 1.39	24.81 ± 1.31	58.5 ± 1.02	26.38 ± 1.43	67.7 ± 1.27	23.31 ± 1.04

Data were represented as mean ± SD ($n = 5$)

Selection of independent variables

Different preliminary trials were carried out (data not shown) to determine various variables impacting the formulation of NPVs. Literature review suggested the significance of drug phospholipid ratio on successful formation of biocompatible adduct through non-covalent bonding and also on solubility, particle charge, permeability across skin membranes, oral bioavailability and stability [25, 62, 63]. Few research groups highlighted that the solvent medium selected should dissolve drug, phospholipid and should be aprotic [21, 64, 65]. While some reported the importance of rotation speed of reflux medium on entrapment efficiency and particle size [66]. Different study groups reported different data with different methods of preparation. In case of solvent evaporation technique, some groups reported the role of duration and temperature of reflux with associated phase transition temperature of phospholipids used, ultimately affecting the successful reaction between drug and phospholipid, partition coefficient, entrapment and stability [24, 67–69]. However, the ratio of drug and phospholipids (Phospholipon® 90H and Lipoid® S100) used in this study was selected based on preliminary trials and their observation (data not shown). Furthermore, the levels for process variables such as reaction duration and temperature were identified by studying their individual and interactive effect on dependent variables—partition coefficient and entrapment efficiency for CGA 90H NPVs and CGA S100 NPVs.

Effect of independent factors (X_1, X_2, X_3) on dependent factors (Y_1 &Y_2)

The polynomial Eqs. (15–18) highlighted the relationship between independent and dependent variables with reiteration in the 3D figures (Fig. 1). The partition coefficient values for CGA 90H NPVs ranged from 0.354 to 1.036, while for CGA S100 NPVs it was 0.560–0.947 as compared to 0.036 of pure CGA. In case of CGA 90H NPVs, a positive significant impact on partition coefficient was obtained with (X_1) drug: phospholipid ratio ($P = 0.050$) and quadratic term (X_1^2) drug: phospholipid ratio($P = 0.0229$). This shows that as the drug phospholipid ratio increases from 1:1 to 1:3, the partition coefficient values also increased. This can be because of higher concentration of phospholipid remain available in uncomplexed form, forming additional layers encircling the NPVs thus rendering a more lipophilic character to them [66, 70]. Further, the interaction term (X_1X_2) drug phospholipid ratio*reaction time influenced partition coefficient in negative manner for CGA 90H NPVs ($P = 0.0430$) and positively for CGA S100 NPVs($P = 0.0021$). This can be attributed to the higher phosphatidylcholine content in LIPOID® S100 (> 94%) which provided more phosphatidylcholine molecules for complexation at higher reaction times yielding a more lipophilic NPV, while Phospholipon® 90H having a comparatively low phosphatidylcholine content, when reacted for longer times, may cause dissociation in the hydrogen bonding between CGA phenolic group and choline moiety of Phospholipon®90H [29].

Also, it has been previously reported that reaction temperatures when kept above the phase transition temperature (> 55 °C) of phospholipid (60 °C used in the present study) will aid in complexation reaction [67, 71]. Similar effect was observed on NPVs partition coefficient values with higher reaction temperature (X_3^2) ($P = 0.0235$ & $P = 0.0428$, respectively).

The entrapment efficiency was found in the range of 66.13%- 99.6% for CGA 90H NPVs and 77.85%-88.0% for CGA S100 NPVs. The independent factors that had a significant effect on entrapment efficiency were (X_1) drug phospholipid ratio($P = 0.0582$) and interaction term (X_1X_3) drug phospholipid ratio*reaction temperature($P = 0.0006$) in case of CGA 90H NPVs. It was observed that higher was the concentration of (X_1) drug phospholipid ratio($P = 0.0582$) higher was entrapment efficiency as more phospholipid was available to complex with CGA [24]. Thus, the optimized value of drug phospholipid ratio for CGA 90H NPV was 1:3.

However, for CGA S100 NPVs, the optimized value was 1:1. This can be attributed to higher phosphatidylcholine content of LIPOID® S100 which gave good entrapment at 1:1 ratio itself [72]. While the interaction term (X_1X_3) drug phospholipid ratio*reaction temperature ($P=0.0006$) highlighted the significance of phase transition temperature of phospholipid and appropriate ratio of drug and phospholipid required for successful formulation of NPV.

In case of CGA S100 NPVs, significant impact on entrapment was obtained with interaction term (X_1X_2) drug phospholipid ratio* reaction time ($P=0.0241$) which gave a negative value attributing to the fact that phospholipid molecules might undergo dissociation at longer reaction time, leading to low entrapment values [29]. Desirability function was used to determine the optimum level of all independent variables to get an optimal response. Figure 2 reports the individual desirability and combined desirability of responses with maximum combined desirability value of 0.905 and 0.943. Thus, it can be concluded that phenolic functional groups present in CGA bonded with choline moiety of phospholipids (Phospholipon® 90H & LIPOID® S100) successfully, depending upon the availability of phosphatidylcholine moieties (drug: phospholipid ratio (1:3 and 1:1, respectively)), at minimum reaction times (1 h) and at higher reaction temperatures (60 °C).

The efficiency of these optimized levels of independent factors was further affirmed with higher Log P values exhibiting higher lipophilic solubility than that of the pure CGA. This improved solubility was confirmed with HPTLC analysis. Furthermore, NPVs obtained with LIPOID® S100 were sticky as compared to free flowing NPVs obtained with Phospholipon® 90H. This was because LIPOID® S100 is a unhydrogenated soyabean phospholipid with higher phosphatidylcholine and linoleic acid content in its composition [72] as compared to hydrogenated soyabean phospholipid—Phospholipon® 90H. This was also one of the causes for lower yield of CGA S100 NPVs as compared to CGA 90H NPVs. However, in terms of particle size, not much difference was obtained with both phospholipids. Both the NPVs gave particle range ≅ 400 nm and PDI values < 0.5 indicating acceptable particle size and monodispersity, which is important for endocytosis dependent cellular uptake and retention in body tissues [48]. The wider particle size distribution can be attributed to employment of soyabean phospholipids in NPV formulation which reportedly result in large particles [73]. These results were also supported by TEM microscopy showing near to spherical structures. The zeta potential values (close to −30 mV for NPVs) indicated the stability of particles in liquid medium while the negative charge on the particles can be attributed to the phospholipids which carry negative charge in a neutral medium [74].

For a successful NPV formulation, phenolic OH groups in CGA has to bind to the choline N [CH_3] and phosphate (P=O) moieties of both the phospholipids. The disappearance and shifting in these wave numbers of these functional groups determined by FTIR indicate hydrogen bonding, van der Waals forces and ion dipole forces between CGA and Phospholipon® 90H/LIPOID® S100 forming NPVs. Similar results were exhibited by DSC and ^{1}H-NMR analysis, with complete disappearance of original excipients peaks [22] and broader signals with characteristic excipients peaks [55] (respectively), suggesting weak intermolecular forces (van der Waals forces and ion dipole forces) between CGA and phospholipids (Phospholipon® 90H/LIPOID® S100).

The formulated hydrogels were semitransparent (CGA 90H NPVs hydrogel) to opaque (CGA S100 NPVs hydrogel) in appearance as compared to transparent hydrogel of pure CGA exhibiting compatibility with skin pH, non-irritancy, stability and optimum viscosity indicating their applicability for topical administration [66]

Dissolution, diffusion and permeation studies

A higher in vitro drug dissolution was obtained with CGA 90H NPVs (98.36 ± 1.02%) as compared to CGA S100 NPVs (94.87 ± 1.34%) for a period of 24 h ($<P=0.001$, Student's t test). The lower dissolution rate can be attributed to the higher phosphatidylcholine content (> 94%) of LIPOID® S100 as compared Phospholipon® 90H which has comparatively lower phosphatidylcholine (< 90%) [72]. Higher phosphatidylcholine content results in more non-covalent bonding between polar groups of CGA and phosphatidyl groups of LIPOID® S100 leading to lower dissolution rate. Figure 8A shows the sustained release of NPVs as compared to pure CGA. CGA being highly soluble, show maximum drug release within the first 8 h. While NPVs show a sustained action over 24 h because of the change in the morphology of crystalline nature of CGA and amphiphilic nature of Phospholipon® 90H & LIPOID® S100 in NPV form [74]. Also, the sustained action of NPVs can be explained with Dash et al. theory [33]. It is assumed that release occurs in two steps—first, CGA dissociates itself from phospholipid and second, the dissociated CGA has to diffuse out of NPV matrix. This theory was affirmed with the release kinetic data of CGA NPVs following Higuchi model based on Fickian diffusion, i.e. dissociation and diffusion [75]. Thus, CGA 90H NPVs and CGA S100 NPVs were found to significantly enhance the rate and extent of dissolution.

Correspondingly, a sustained diffusion of CGA from CGA 90H NPVs hydrogel (101.9 ± 1.12%) and CGA S100 NPVs hydrogel (99.9 ± 1.64%) for a period of 48 h

was obtained ($<P=0.001$, Student's t test). Figure 8B shows rapid cumulative drug diffusion of CGA from CGA hydrogel within the first 10 h, as being highly soluble, just diffused out the Carbopol matrix. While Simon et al. explained the sustained drug diffusion mechanism of NPVs hydrogel through porous dialysis membrane as a multiple step process [76], where the CGA NPVs first lodges themselves in the porous dialysis membrane; then CGA dissociates itself from phospholipid; and lastly the dissociated CGA has to diffuse out of NPVs matrix and Carbopol matrix subsequently. Thus, the highest cumulative drug diffusion obtained with CGA hydrogel (88.1 ± 1.32%) was within the first 10 h as compared to superior and sustained release pattern of CGA 90H NPVs and CGA S100 NPVs hydrogel, reflecting the efficiency of these formulations.

Additionally, the ex vivo permeation studies provided an astute understanding of the in vivo performance of NPVs hydrogel formulations. CGA being highly polar with multiple ring structure and large particle size was unable to cross the biological membrane via intercellular transport, thus giving lower cumulative permeation (14.63 ± 1.15%). While amphiphilic CGA 90H NPVs (32.49 ± 1.16%) and CGA S100 NPVs (31.98 ± 1.21%) were able to transition themselves easily between the lipophilic and hydrophilic barrier of biological membrane giving higher cumulative permeation values (Fig. 8C) [77]. These results were further supported by higher steady-state flux and permeability coefficient values with a slightly higher values for CGA 90H NPVs hydrogel as compared to CGA S100 NPVs hydrogel. A possible explanation for this can be difference in the phospholipid used and its ability to dissociate the drug for further diffusion through the skin membrane. These results were further substantiated by CLSM microscopy, where fluorescence obtained with CGA 90H NPVs RHO hydrogel and CGA S100 NPVs RHO hydrogel was evenly distributed throughout the skin tissue, indicating higher permeability.

In vitro antioxidant and cell viability study

When afflicted with any pathological condition, body generates tons of free radicals which damage biological membranes leading to clinical expression of many diseases [78]. Also overload of ions like iron result in DNA damage and neurodegeneration [79]. Phenolic compounds like CGA have the ability to reduce the free radicals and chelate these ions [17]. The Fe^{2+} chelation ability was assessed using colorimetric method based on the plot that Fe^{2+} forms a bond with ferrozine to give a bluish coloured metallic complex, which can be measured spectrophotometrically; however, in the presence of CGA there is disruption in formation of this metallic complex causing decreased absorbance values [38]. The reduction in absorbance values was reported in percentage with CGA S100 NPVs (78.12 ± 0.86%) showing higher Fe^{2+} chelation ability with lower percentage as compared to CGA 90H NPVs (80.36 ± 0.19%). Also, the ability to reduce free radicals was evaluated spectrophotometrically by measuring the absorbance of DPPH with increasing concentration of CGA (20–200 µg/mL). CGA donates hydrogen atoms to reduce free radical DPPH to its non-radical form resulting in decrease of absorbance values, reported as per cent radical scavenged [80]. Herein, CGA 90H NPVs showed higher percentage of radicals scavenged (96.74 ± 0.09%) as compared to CGA S100 NPVs (95.12 ± 0.86%). This difference can be attributed to the release of CGA from NPVs matrix affecting their activity. Furthermore, reports have shown that phosphatidylcholine, having choline head group and intermolecular hydroxyl groups in its structure, itself acts as antioxidant [81]. Thus, enhanced antioxidant activity of NPVs as compared to pure CGA was due to synergistic effect of formulation components (CGA and phospholipids).

The cell viability in HeLa and HL-60 cell lines was screened with CGA 90H NPVs and CGA S100 NPVs by MTT assay [82]. Previous reports suggested that with HL-60, downregulation of apoptosis-related proteins such as Akt inhibit proliferation and induce apoptosis [83], while the cytotoxic effect of CGA in HeLa cells is due to the prooxidant nature causing intermolecular production of ROS at higher concentrations having a high cytotoxic potency [40]. The NPVs were able to reduce the viability in both the cell lines in a dose-dependent manner with lower IC_{50} values as compared to pure CGA(0.75 times lower). While longer exposure resulted in additional toxicity to the cells (Fig. 11C–D), demonstrating a dose- and time-dependent activity. This decrease in the cell viability in both the cell lines can be attributed to the amount of CGA entrapped in CGA 90H NPV and CGA S100 NPV and its release from the respective NPV matrix, which also accounts for the difference obtained with the two NPVs. The results obtained highlight the efficiency of CGA NPVs formulation in anticancer activity.

Pharmacodynamic study: wound-healing activity

Phenolic derivative like CGA, with a potent wound-healing activity, is limited by its low permeability because of high polarity and multiple ring structure resulting in larger particle size [16]. But with NPVs, the permeability improved more than 2 folds with improved physicochemical properties like lower particle size (≅400 nm) and PDI values (<0.5). It was evident with CGA 90H NPVs and CGA S100 NPVs hydrogels which depicted higher reduction in wound area and percentage wound contraction as compared to CGA hydrogel or Silverex® heal marketed

hydrogel, because of their lower particle size and PDI values (437.6 ± 31 nm and 449.6 ± 24.9 nm with PDI values 0.436 and 0.489, respectively). It has been reported that NPVs are able to cross upper stratum corneum intercellularly and traverse across skin layers by maintaining a concentration gradient and simultaneously release drug in a sustained pattern [16]. A relatively higher wound-healing activity was obtained with CGA S100 NPVs hydrogel, which was in contradiction to its permeability results. This enhanced in vivo permeability of CGA S100 NPVs hydrogel can be attributed to the phospholipid component LIPOID® S100, which mimicked the biomembranes [84]. Additionally, it was observed that the wound-healing process was supplemented by the ability of CGA to reduce oxidative stress in a wound tissue [44]. Thus, CGA 90H NPVs and CGA S100 NPVs with their evident enhanced antioxidant activity were more efficient than pure CGA in healing wound.

Pharmacokinetic study: oral bioavailability studies

A significant increase in oral bioavailability was obtained with CGA 90H NPVs and CGA S100 NPVs as compared to pure CGA. Different reasons attribute to this increase in bioavailability such as, firstly, improved physicochemical properties of CGA NPVs as compared to pure CGA, like higher Log P values which imply the increased lipophilic solubility of CGA in NPV form. Lipophilic nature of NPVs helps them fuse in between biomembranes, which are mainly composed of phospholipid and proteins [85] and thus easy transportation of CGA NPVs into cells. Secondly, CGA has been previously reported to get quickly metabolized in intestine [86]. It was also evident through the AUC values obtained with CGA (~ 110.43 µg/mL*h) which indicated reabsorption of CGA in hepato-enteral circulation [18]. While the *AUC* and $t_{1/2}$ values exhibited by CGA 90H NPVs and CGA S100 NPVs((~ 327.23 µg/mL*h and ~ 183.85 µg/mL*h and 25.87 h and 22.53 h, respectively) suggested their entry in systemic circulation with prevention of first pass metabolism and better transitioning between intestinal membranes with increased absorption [87]. It was further observed that as compared to groups treated with CGA 90H NPVs, groups treated with CGA S100 NPVs gave lower as *Cmax, Tmax and AUC* values. The possible explanation for this lies in the phosphatidylcholine content of LIPOID® S100, which is reported to have negative effect on its absorption [72]. However, the ability of LIPOID® S100 to mimic biomembranes was advantageous and could be seen with higher volume of distribution (*Vz/F*) (3.79 mg/µg/ml^{-1} with CGA S100 NPVs) value as compared to CGA 90H NPVs (2.09 mg/µg/ml^{-1}).

Additionally, a comparison between in vitro per cent drug release and in vivo per cent drug absorbed for a period of 8 h was studied by applying model-independent Wagner–Nelson method [76, 88]. The results (Table 8) obtained implied that in vitro dissolution studies served as a representative understudy for in vivo bioavailability with slightly overlayered plots (single point) exhibiting sustained in vitro release and in vivo absorbed values for CGA 90H NPVs and CGA S100 NPVs. While with pure CGA, rapid in vitro drug release within 8 h indicating its highly soluble nature and lower in vivo absorption values within 0.5 h indicating low half-life of pure CGA, showed no over layering in IVIV plot.

Conclusion

The phenolic derivative, CGA, was successfully formulated and optimized as NPVs, revealing their efficiency for improving the lipophilic solubility, permeability, oral bioavailability, stability and ultimately enhancing their antioxidant, anticancer and wound-healing potentials. The data obtained from FTIR, DSC, ^{1}H-NMR clearly showed the presence of non-covalent bonding, i.e. hydrogen bonding, van der Waals and dipole–dipole interactions between CGA and phospholipids (Phospholipon® 90H and Lipoid® S100). Solubility studies demonstrated higher lipophilic solubility supported by higher Rf values in HPTLC studies. Both the formulations were found to be stable with negligible changes in partition coefficient, entrapment efficiency and zeta potential values for a period of 6 months. The phosphatidylcholine content of Phospholipon® 90H and Lipoid® S100 used for formulating NPV affected the properties and overall performance of CGA 90H NPVs and CGA S100 NPVs. CGA 90H NPVs performed better with in vitro and ex vivo permeability studies as compared to higher permeability of CGA S100 NPVs in vivo (wound-healing studies). On the other hand, CGA 90H NPVs performed better in vivo oral bioavailability studies with higher *C*max, *T*max, $t_{1/2}$ and AUC values as compared to CGA S100 NPVs. Further studies are required to evaluate correlation between *IVIV* with different compartment modelling. Overall, promising results from this first of its kind study affirmed that the formulated CGA 90H NPVs and CGA S100 NPVs offer an effective delivery system for enhancing biopharmaceutical and pharmacological potential of CGA.

Abbreviations

CGA	Chlorogenic acid
BCS	Biopharmaceutical classification system
NPVs	Nanophytovesicles
CGA 90H NPVs	Chlorogenic acid Phospholipon® 90H nanophytovesicles
CGA S100 NPVs	Chlorogenic acid Lipoid® S100 nanophytovesicles
DPPH	2-Diphenyl-1-picrylhydrazyl
MTT	3-(4,5-Dimethylthiazol-2-yl)- 2,5- diphenyltetrazolium bromide
RHO	Rhodamine 6G

MEM	Minimum Essential Medium Eagle medium
RPMI-1640	Roswell Park Memorial Institute Medium
FBS	Foetal bovine serum
HL-60	Human leukaemia cell line
HeLa	Henrietta Lacks cervical cancer cell line
CCD	Central composite design
CLSM	Confocal fluorescence microscopy
IVIVC	In vitro in vivo correlation
PDI	Polydispersity index
TEM	Transmission electron microscopy

Acknowledgements
The authors express their gratitude to Department of Pharmaceutical Sciences, R.T.M. Nagpur University for providing facilities. The authors are grateful to Dr. Manoj Upadhya, Aston Pharmacy School and Neuroscience, Aston University for his help in carrying out confocal microscopy. The authors also acknowledge LIPOID GmbH Germany for providing the gift sample of Phospholipon® 90H and Lipoid® S100 for the research study.

Author contributions
HT and PP both contributed to the study conception and design. Methodology, data collection, data analysis and writing of the original draft were performed by HT. While supervision, material procurement and facility support were provided by PP. Both the authors read and approved the final manuscript.

Funding
The current study received no funding from government agencies.

Availability of data and materials
The data that support the findings of this study are available from the corresponding author, upon reasonable request.

Declarations

Ethics approval and consent to participate
The animal protocols were approved by institutional animal ethics committee of Central animal house, Department of pharmaceutical Sciences, R.T.M. Nagpur University (IAEC/UDPS/2020/47, dated 4th of August 2018) and the laboratory animal license number is 92/PO/Re/S/99/CPCSEA. The studies were performed according to the ethical guidelines of Committee for Purpose of Control and Supervision of Experiments on Animals (CPCSEA). Sprague Dawley rats (220–230 g) were procured from Central animal house, Department of pharmaceutical Sciences, R.T.M. Nagpur University and housed in controlled environment. The rats were segregated and labelled accordingly with acclimatization period of minimum 7 days. A 12 h light and dark cycle was maintained with standard diet and water ad libitum during all periods.

Consent for publication
The authors declare no conflict of interest.

Competing interests
The authors declare that they have no conflict of interest.

Author details
[1]Department of Pharmaceutical Sciences, Rashtrasant Tukadoji Maharaj Nagpur University, Nagpur, Maharashtra 440033, India.

Received: 4 August 2023 Accepted: 12 November 2023
Published online: 13 December 2023

References

1. Raskar V, Bhalekar MR (2019) Formulation of coffee bean extract (chlorogenic acid) solid lipid nanoparticles for lymphatic uptake on oral administration. J Drug Deliv Therap. 9(4):477–484
2. Elisha IL, Botha FS, McGaw LJ, Eloff JN (2017) The antibacterial activity of extracts of nine plant species with good activity against Escherichia coli against five other bacteria and cytotoxicity of extracts. BMC Complement Altern Med 17(1):133
3. Rosas-Cruz GP, Silva-Correa CR, Calderón- Peña AA, Villarreal-La Torre VE, Aspajo-Villalaz CL, Cruzado-Razco JL et al (2020) Wound healing Activity of an Ointment from *Solanum tuberosum* L. "Tumbay Yellow Potato" on Mus musculus Balb/c. Pharmacognosy J 12(6):1268–1275
4. Chen WC, Liou SS, Tzeng TF, Lee SL, Liu IM (2012) Wound repair and anti-inflammatory potential of Lonicera japonica in excision wound-induced rats. BMC Complement Altern Med 12:226
5. Nagar HK, Srivastava AK, Srivastava R, Kurmi ML, Chandel HS, Ranawat MS (2016) Pharmacological investigation of the wound healing activity of *Cestrum nocturnum* (L.) ointment in Wistar albino rats. J Pharm (Cairo). 2016:9249040
6. Paswan SK, Srivastava S, Rao CV (2020) Wound healing, antimicrobial and antioxidant efficacy of Amaranthus spinosus ethanolic extract on rats. Biocatal Agric Biotechnol 26:101624
7. Moghadam SE, Ebrahimi SN, Salehi P, MoridiFarimani M, Hamburger M, Jabbarzadeh E (2017) Wound Healing Potential of Chlorogenic Acid and Myricetin-3-O-beta-Rhamnoside Isolated from Parrotia persica. Molecules 22(9):1501
8. Mitrea D-R, Malkey R, Pop N-L, Filip A, Clichici S, Moldovan R et al (2020) Single oral dose of chlorogenic acid attenuates the experimental carrageenan-induced oxidative stress. Health Sport Rehabil 21:74–81
9. Nie X, Chen Z, Pang L, Wang L, Jiang H, Chen Y et al (2020) Oral nano drug delivery systems for the treatment of type 2 diabetes mellitus: an available administration strategy for antidiabetic phytocompounds. Int J Nanomedicine 15:10215–10240
10. Zhu S, Shen Y, Yu Y, Bai X (2020) Synthesis of antibacterial gold nanoparticles with different particle sizes using chlorogenic acid. R Soc Open Sci 7(3):191141
11. Lu H, Tian Z, Cui Y, Liu Z, Ma X (2020) Chlorogenic acid: A comprehensive review of the dietary sources, processing effects, bioavailability, beneficial properties, mechanisms of action, and future directions. Compr Rev Food Sci Food Saf 19(6):3130–3158
12. Liang N, Kitts DD (2015) Role of chlorogenic acids in controlling oxidative and inflammatory stress conditions. Nutrients 8(1):16
13. Parmar KM, Shende PR, Katare N, Dhobi M, Prasad SK (2018) Wound healing potential of Solanum xanthocarpum in streptozotocin-induced diabetic rats. J Pharm Pharmacol 70(10):1389–1400
14. Zhou Y, Zhou T, Pei Q, Liu S, Yuan H (2014) Pharmacokinetics and tissue distribution study of chlorogenic acid from lonicerae japonicae flos following oral administrations in rats. Evid Based Complement Alternat Med 2014:979414
15. Narita Y, Inouye K (2013) Degradation kinetics of chlorogenic acid at various pH values and effects of ascorbic acid and epigallocatechin gallate on its stability under alkaline conditions. J Agric Food Chem 61(4):966–972
16. Alharbi WS, Almughem FA, Almehmady AM, Jarallah SJ, Alsharif WK, Alzahrani NM et al (2021) Phytosomes as an emerging nanotechnology platform for the topical delivery of bioactive phytochemicals. Pharmaceutics 13(9):1475
17. Bhattacharyya S, Majhi S, Saha BP, Mukherjee PK (2014) Chlorogenic acid-phospholipid complex improve protection against UVA induced oxidative stress. J Photochem Photobiol B 130:293–298
18. Li Y, Ren X, Lio C, Sun W, Lai K, Liu Y et al (2018) A chlorogenic acid-phospholipid complex ameliorates post-myocardial infarction inflammatory response mediated by mitochondrial reactive oxygen species in SAMP8 mice. Pharmacol Res 130:110–122
19. Feng Y, Sun C, Yuan Y, Zhu Y, Wan J, Firempong CK et al (2016) Enhanced oral bioavailability and in vivo antioxidant activity of chlorogenic acid via liposomal formulation. Int J Pharm 501(1–2):342–349
20. Nallamuthu I, Devi A, Khanum F (2015) Chlorogenic acid loaded chitosan nanoparticles with sustained release property, retained antioxidant activity and enhanced bioavailability. Asian J Pharm Sci 10(3):203–211
21. Kuche K, Bhargavi N, Dora CP, Jain S (2019) Drug-phospholipid complex-a go through strategy for enhanced oral bioavailability. AAPS PharmSciTech 20(2):43
22. Saoji SD, Raut NA, Dhore PW, Borkar CD, Popielarczyk M, Dave VS (2016) Preparation and evaluation of phospholipid-based complex of

standardized centella extract (SCE) for the enhanced delivery of phyto-constituents. AAPS J 18(1):102–114
23. Singh C, Bhatt TD, Gill MS, Suresh S (2014) Novel rifampicin-phospholipid complex for tubercular therapy: synthesis, physicochemical characterization and in-vivo evaluation. Int J Pharm 460(1–2):220–227
24. Das M, Kalita B (2014) Design and evaluation of phyto-phospholipid complexes (phytosomes) of rutin for transdermal application. J Appl Pharm Sci 4:51–57
25. Molaveisi M, ShahidiNoghabi M, Parastouei K, Taheri RA (2021) Fate of nano-phytosomes containing bioactive compounds of Echinacea extract in an acidic food beverage. Food Struct 27:100177
26. Telange D, Patil A, Pethe A, Tatode A, Sridhar A, Dave V (2016) Kaempferol-phospholipid complex: formulation, and evaluation of improved solubility, in vivo bioavailability, and antioxidant potential of kaempferol. J Excip Food Chem 7:89
27. Habbu P, Madagundi S, Kulkarni R, Jadav S, Vanakudri R, Kulkarni V (2013) Preparation and evaluation of Bacopa–phospholipid complex for antiamnesic activity in rodents. Drug Invention Today 5(1):13–21
28. Shete VS, Telange DR, Mahajan NM, Pethe AM, Mahapatra DK (2023) Development of phospholipon®90H complex nanocarrier with enhanced oral bioavailability and anti-inflammatory potential of genistein. Drug Delivery 30(1):2162158
29. Beg S, Raza K, Kumar R, Chadha R, Katare OP, Singh B (2016) Improved intestinal lymphatic drug targeting via phospholipid complex-loaded nanolipospheres of rosuvastatin calcium. RSC Adv 6(10):8173–8187
30. Chong YK, Zainol I, Ng CH, Ooi IH (2019) Miktoarm star polymers nanocarrier: synthesis, characterisation, and in-vitro drug release study. J Polym Res 26(3):79
31. Vu T-T-G, Nguyen H-T, Yen T, Pham B-T, Pham T-M-H (2021) Preparation and physicochemical evaluation of hydrogel containing quercetin phytosomes. Pharmaceutical Sciences Asia 48:122–138
32. Sugiyama M, Akita M, Alépée N, Fujishiro M, Hagino S, Handa Y et al (2018) Comparative assessment of 24-hr primary skin irritation test and human patch test data with in vitro skin irritation tests according to OECD Test Guideline 439 (for quasi-drugs in Japan). J Toxicol Sci 43(12):751–768
33. Dash S, Murthy PN, Nath L, Chowdhury P (2010) Kinetic modeling on drug release from controlled drug delivery systems. Acta Pol Pharm 67(3):217–223
34. Telange DR, Nirgulkar SB, Umekar MJ, Patil AT, Pethe AM, Bali NR (2019) Enhanced transdermal permeation and anti-inflammatory potential of phospholipids complex-loaded matrix film of umbelliferone: formulation development, physico-chemical and functional characterization. Eur J Pharm Sci 131:23–38
35. Georgescu M, Marinas O, Popa M, Stan T, Lazar V, Bertesteanu SV, et al. Natural Compounds for Wound Healing. Worldwide Wound Healing - Innovation in Natural and Conventional Methods 2016
36. Eltoum I, Fredenburgh J, Grizzle WE (2001) Advanced Concepts in Fixation: 1. effects of fixation on immunohistochemistry, reversibility of fixation and recovery of proteins, nucleic acids, and other molecules from fixed and processed tissues. 2. Developmental methods of fixation. J Histotechnol 24(3):201–210
37. ICH (2003) International Conference on Harmonisation; Stability Data Package for Registration Applications in Climatic Zones III and IV; Stability Testing of New Drug Substances and Products; availability. Notice. Fed Regist. 68(225):65717–8.
38. Yang R, Tian J, Liu Y, Zhu L, Sun J, Meng D et al (2021) Interaction mechanism of ferritin protein with chlorogenic acid and iron ion: The structure, iron redox, and polymerization evaluation. Food Chem 349:129144
39. Santos JS, AlvarengaBrizola VR, Granato D (2017) High-throughput assay comparison and standardization for metal chelating capacity screening: A proposal and application. Food Chem 214:515–522
40. Krstic M, Stojadinovic M, Smiljanic K, Stanic-Vucinic D, CirkovicVelickovic T (2015) The anti-cancer activity of green tea, coffee and cocoa extracts on human cervical adenocarcinoma HeLa cells depends on both pro-oxidant and anti-proliferative activities of polyphenols. RSC Adv 5(5):3260–3268
41. Catanzaro D, Filippini R, Vianello C, Carrara M, Ragazzi E, Montopoli M (2016) Chlorogenic acid interaction with cisplatin and oxaliplatin: studies in cervical carcinoma cells. Nat Prod Commun 11(4):499–502
42. Riss TL, Moravec RA, Niles AL, Duellman S, Benink HA, Worzella TJ et al (2004) Cell Viability Assays. In: Markossian S, Grossman A, Brimacombe K, Arkin M, Auld D, Austin C et al (eds) Assay Guidance Manual. Eli Lilly & Company and the National Center for Advancing Translational Sciences, Bethesda
43. Bovill J (2008) Inhalation anaesthesia: from diethyl ether to xenon. Handbook Exp Pharmacol. 182:121–142
44. Chen WC, Liou SS, Tzeng TF, Lee SL, Liu IM (2013) Effect of topical application of chlorogenic acid on excision wound healing in rats. Planta Med 79(8):616–621
45. Dons T, Soosairaj S (2018) Evaluation of wound healing effect of herbal lotion in albino rats and its antibacterial activities. Clin Phytosci 4(1):6
46. Nair B (2019) Clinical Trial Designs. Indian Dermatol Online J. 10(2):193–201
47. Farrell TL, Dew TP, Poquet L, Hanson P, Williamson G (2011) Absorption and metabolism of chlorogenic acids in cultured gastric epithelial monolayers. Drug Metab Dispos 39(12):2338–2346
48. Danaei M, Dehghankhold M, Ataei S, HasanzadehDavarani F, Javanmard R, Dokhani A et al (2018) Impact of particle size and polydispersity index on the clinical applications of lipidic nanocarrier systems. Pharmaceutics 10(2):57
49. Honary S, Zahir F (2013) Effect of zeta potential on the properties of nano-drug delivery systems - a review (part 1). Trop J Pharm Res 12(2):265–273
50. Liang N, Lu X, Hu Y, Kitts DD (2016) Application of attenuated total reflectance-fourier transformed infrared (ATR-FTIR) spectroscopy to determine the chlorogenic acid isomer profile and antioxidant capacity of coffee beans. J Agric Food Chem 64(3):681–689
51. Chao J, Wang H, Zhao W, Zhang M, Zhang L (2012) Investigation of the inclusion behavior of chlorogenic acid with hydroxypropyl-β-cyclodextrin. Int J Biol Macromol 50(1):277–282
52. Cai X, Luan Y, Jiang Y, Song A, Shao W, Li Z et al (2012) Huperzine A-phospholipid complex-loaded biodegradable thermosensitive polymer gel for controlled drug release. Int J Pharm 433(1–2):102–111
53. Chewchida S, Vongsak B (2019) Simultaneous HPTLC quantification of three caffeoylquinic acids in Pluchea indica leaves and their commercial products in Thailand. Rev Bras 29(2):177–181
54. Wagner H, Bauer R, Melchart D, Xiao P-G, Staudinger A. Chromatographic Fingerprint Analysis of Herbal Medicines: Thin-layer and High Performance Liquid Chromatography of Chinese Drugs 2015. 1–267 p
55. Marković S, Tošović J, DimitrićMarković JM (2016) Synergic application of spectroscopic and theoretical methods to the chlorogenic acid structure elucidation. Spectrochim Acta A Mol Biomol Spectrosc 164:67–75
56. Lipoid. PHOSPHOLIPON® 90 H & LIPOID S100 2013 [Available from: http://www.bashiraz.com/images/products/Lipoid_List.pdf.
57. Nyigo V, Mdegela R, Mabiki F, Malebo H (2015) Assessment of dermal irritation and acute toxicity potential of extracts from synadenium glaucescens on healthy rabbits, wistar albino rats and albino mice. Eur J Med Plants. 10(4):1–11
58. Shi G, Rao L, Yu H, Xiang H, Pen G, Long S et al (2007) Yeast-cell-based microencapsulation of chlorogenic acid as a water-soluble antioxidant. J Food Eng 80(4):1060–1067
59. Chang q, Zuo Z, Chow M, Ho W, (2006) Effect of storage temperature on phenolics stability in hawthorn (Crataegus pinnatifida var. major) fruits and a hawthorn drink. Food Chemistry - FOOD CHEM 98:426–430
60. Zbuchea A, Lungu L, Popa CV, Tecuceanu V, Alexandru VB, Tatia R, editors. An Innovative Ointment Made of Natural Ingredients with Increased Wound Healing Activity 2016.
61. Bhattacharya S. Central Composite Design for Response Surface Methodology and Its Application in Pharmacy. 2021. p. 1–19.
62. Khan J, Alexander A, Ajazuddin SS, Saraf S (2013) Recent advances and future prospects of phyto-phospholipid complexation technique for improving pharmacokinetic profile of plant actives. J Control Release 168(1):50–60
63. Ajazuddin SS (2010) Applications of novel drug delivery system for herbal formulations. Fitoterapia 81(7):680–689
64. Lu M, Qiu Q, Luo X, Liu X, Sun J, Wang C et al (2019) Phyto-phospholipid complexes (phytosomes): A novel strategy to improve the bioavailability of active constituents. Asian J Pharm Sci 14(3):265–274

65. Tan Q, Liu S, Chen X, Wu M, Wang H, Yin H et al (2012) Design and evaluation of a novel evodiamine-phospholipid complex for improved oral bioavailability. AAPS PharmSciTech 13(2):534–547
66. Taleuzzaman M, Sartaj A, Kumar Gupta D, Gilani SJ, Mirza MA (2023) Phytosomal gel of Manjistha extract (MJE) formulated and optimized with central composite design of Quality by Design (QbD). J Dispersion Sci Technol 44(2):236–244
67. Pathan RA, Bhandari U (2010) Preparation & characterization of embelin–phospholipid complex as effective drug delivery tool. J Incl Phenom Macrocycl Chem 69(1–2):139–147
68. Trivedi H, Puranik PK (2022) Antibacterial activity of chlorogenic acid phytovesicles against resistant bacteria: development, optimization and evaluation. Int J Appl Pharm 14(1):83–92
69. Alhakamy NA, Fahmy UA, Eldin SMB, Ahmed OAA, Aldawsari HM, Okbazghi SZ et al (2021) Scorpion venom-functionalized quercetin phytosomes for breast cancer management: in vitro response surface optimization and anticancer activity against MCF cells. Polym (Basel) 14(1):93
70. GuimarãesSáCorreia M, Briuglia ML, Niosi F, Lamprou DA (2017) Microfluidic manufacturing of phospholipid nanoparticles: Stability, encapsulation efficacy, and drug release. Int J Pharm 516(1):91–99
71. Udapurkar PP, Bhusnure OG, Kamble SR (2018) Diosmin phytosomes: development, optimization and physicochemical characterization. Indian J Pharm Edu Res 52(4s):s29–s36
72. Xianchuang W (2015) Bioavailability of 10-hydroxycamptothecin-phospholipid complex loaded by solid dispersion and lipid-based formulations. J Chin Pharm Sci 24(12):779–787
73. Vergara D, Shene C (2019) Encapsulation of lactoferrin into rapeseed phospholipids based liposomes: optimization and physicochemical characterization. J Food Eng 262:29–38
74. Telange DR, Patil AT, Pethe AM, Fegade H, Anand S, Dave VS (2017) Formulation and characterization of an apigenin-phospholipid phytosome (APLC) for improved solubility, in vivo bioavailability, and antioxidant potential. Eur J Pharm Sci 108:36–49
75. Salome Amarachi C, Onunkwo G, Onyishi I (2013) Kinetics and mechanisms of drug release from swellable and non swellable matrices: a review. Res J Pharm, Biol Chem Sci 4:97–103
76. Simon A, Amaro MI, Healy AM, Cabral LM, de Sousa VP (2016) Comparative evaluation of rivastigmine permeation from a transdermal system in the Franz cell using synthetic membranes and pig ear skin with in vivo-in vitro correlation. Int J Pharm 512(1):234–241
77. Allam AN, Komeil IA, Abdallah OY (2015) Curcumin phytosomal softgel formulation: Development, optimization and physicochemical characterization. Acta Pharm 65(3):285–297
78. Miura T (2015) The peroxidase activity of ADM-Fe3+ cooperates with lipid peroxidation: the participation of hydroperoxide and hydroxyl radicals in the damage to proteins and DNA. Chem Biol Interact 236:67–73
79. Bettencourt C, Forabosco P, Wiethoff S, Heidari M, Johnstone DM, Botía JA et al (2016) Gene co-expression networks shed light into diseases of brain iron accumulation. Neurobiol Dis 87:59–68
80. Zheng L, Lin L, Su G, Zhao Q, Zhao M (2015) Pitfalls of using 1,1-diphenyl-2-picrylhydrazyl (DPPH) assay to assess the radical scavenging activity of peptides: Its susceptibility to interference and low reactivity towards peptides. Food Res Int 76:359–365
81. Saito H, Ishihara K (1997) Antioxidant activity and active sites of phospholipids as antioxidants. J Am Oil Chem Soc 74(12):1531–1536
82. Jiang X, Lu C, Tang M, Yang Z, Jia W, Ma Y et al (2018) Nanotoxicity of silver nanoparticles on HEK293T cells: a combined study using biomechanical and biological techniques. ACS Omega 3(6):6770–6778
83. Liu YJ, Zhou CY, Qiu CH, Lu XM, Wang YT (2013) Chlorogenic acid induced apoptosis and inhibition of proliferation in human acute promyelocytic leukemia HL60 cells. Mol Med Rep 8(4):1106–1110
84. Benson HAE (2006) Transfersomes for transdermal drug delivery. Expert Opin Drug Deliv 3(6):727–737
85. Kell DB (2015) What would be the observable consequences if phospholipid bilayer diffusion of drugs into cells is negligible? Trends Pharmacol Sci 36(1):15–21
86. Wang W, He X, Ma C (2013) Metabolism schemes of chlorogenic, quinic and caffeic acid derivatives in rats deduced by molecular fragments detected with optimized UPLC–APCI-MS/MS conditions. Int J Mass Spectrom 337:34–42
87. Ren T, Wang Y, Wang C, Zhang M, Huang W, Jiang J et al (2017) Isolation and identification of human metabolites from a novel anti-tumor candidate drug 5-chlorogenic acid injection by HPLC-HRMS/MS(n) and HPLC-SPE-NMR. Anal Bioanal Chem 409(30):7035–7048
88. Cheng C, Wu P-C, Lee H-Y, Hsu K-Y (2014) Development and validation of an in vitro–in vivo correlation (IVIVC) model for propranolol hydrochloride extended-release matrix formulations. J Food Drug Anal 22(2):257–263

Publisher's Note